Dominant aerosol chemical components and their contribution to extinction during the Aerosols99 cruise across the Atlantic

P. K. Quinn,[1,2] D. J. Coffman,[1,2] T. S. Bates,[1,2] T. L. Miller,[1,2]
J. E. Johnson,[1,2] K. Voss,[3] E. J. Welton,[4] and C. Neusüss[5]

Abstract. The Aerosols99 cruise crossed the Atlantic Ocean from Norfolk, Virginia, to Cape Town, South Africa, during January and February of 1999. On the basis of back trajectories, aerosol number concentrations and size distributions, and trace gas concentrations, seven "air mass" regions were encountered. These included North America, Northern Hemisphere (NH) marine, African dust, a mixture of dust and biomass burning from Africa, biomass burning from Africa, Southern Hemisphere (SH) marine tropics, and SH marine temperate. Simultaneous measurements of aerosol chemical composition, number size distribution, scattering and absorption coefficients, vertical profiles, and optical depth allowed for a thorough characterization of the aerosol. Presented here are the concentrations and mass fractions of the aerosol chemical components that were dominant in each region and the aerosol scattering and absorption coefficients, single scattering albedos, Ångström exponents, and optical depths measured in each region. Also presented is the percent of the extinction measured at the surface due to each chemical component and mass extinction efficiencies of the individual aerosol components estimated from Mie calculations and a multiple linear regression. All results are reported at the measurement relative humidity of $55 \pm 5\%$. Non-sea-salt (nss) $SO_4^=$ aerosol was a significant contributor to the submicron mass concentration in all air mass regions (mean mass fractions ranged from 20 to 67%). It made the largest contribution to submicron extinction in the North America region ($45 \pm 30\%$, mean and 1σ standard deviation). Sea-salt mean submicron mass fractions ranged from 9 to 49% with the lowest value in the biomass burning region and highest values in the NH marine and dust regions. Its contribution to submicron extinction ranged from a mean of 29 to 66%. Sea-salt mean supermicron mass fractions ranged from 52 to 98% with the highest values in the marine regions. Its contribution to supermicron extinction ranged from 60 to 98%. Mean submicron and supermicron mass fractions of dust in the dust region were $22 \pm 3.3\%$ (mean and 95% uncertainty) and $26 \pm 3.9\%$, respectively. Corresponding submicron and supermicron extinction contributions were 24 ± 7.5 and $18 \pm 4.0\%$, respectively. Submicron mass fractions of particulate organic matter (POM) ranged from below detection limits in the dust region to $18 \pm 11\%$ in the biomass burning region. Contributions to submicron extinction ranged from below detection limits to 24% in the North America region. In the biomass burning region the black carbon mean submicron mass fraction was $6.7 \pm 1.3\%$ with a contribution of $6.4 \pm 2.7\%$ to the submicron extinction. Extinction fractions of each component for particles with aerodynamic diameters less than 10 μm also are reported in the paper. Sea salt dominated the extinction measured at the surface due to sub-10 μm aerosol for all air mass regions, even those influenced by continental sources. The fraction of the measured column aerosol optical depth due to aerosol within the boundary layer was estimated for the NH marine, dust, biomass burning, and SH marine tropics regions. Mean values ranged from $35 \pm 15\%$ for the biomass burning region to $95 \pm 46\%$ for the NH marine region.

[1]Pacific Marine Environmental Laboratory, NOAA Seattle, Washington.

[2]Joint Institute for the Study of the Atmosphere and Ocean, University of Washington, Seattle, Washington.

[3]University of Miami, Miami, Florida.

[4]Goddard Earth Science and Technology Center, University of Maryland, Greenbelt, Maryland.

[5]Institute for Tropospheric Research, Leipzig, Germany.

1. Introduction

It is well known that radiative forcing by tropospheric aerosols is one of the largest uncertainties in model calculations of climate forcing [*Intergovernmental Panel on Climate Change (IPCC)*, 1996]. This is due, in large part, to regionally varying aerosol sources, concentrations, and compositions and the difficulty of making the required in situ measurements of relevant aerosol properties on a global scale. One approach for characterizing aerosol properties over large geographical regions is shipboard cruises with aerosol instrumentation capable of characterizing both surface and column properties (in situ instrumentation for the measurement of aerosol chemical, physical, and optical properties; a sunphotometer for the measurement of aerosol optical depth; and a lidar for the measurement of aerosol vertical profiles). The Aerosols99 cruise was a diagonal transect across the Atlantic Ocean leaving Norfolk, Virginia, on January 14, 1999, and arriving in Cape Town, South Africa, on February 8, 1999. A goal of the cruise was to characterize the aerosol over regions of the Atlantic Ocean known to be impacted by continental emissions and over regions thought to be relatively pristine. In situ measurements of aerosol chemical composition and light scattering and absorption coupled with air mass back trajectories confirm that a wide range of aerosol types were encountered. These included aerosol from eastern North America, dust and biomass burning aerosol from Africa, and marine aerosol from the North and South Atlantic.

On the basis of back trajectories, aerosol number concentrations and size distributions, and trace gas concentrations, samples collected along the cruise track were divided into seven regions that reflect the recent history of the sampled air masses. These "air mass" regions and their latitude and longitude bounds are North America (37°N to 31°N; 76.2°W to 65.8°W), Northern Hemisphere (NH) marine (31°N to 15.5°N; 65.8°W to 43.3°W), African dust (15.5°N to 8°N; 43.3°W to 32.9°W), mixture of African dust and biomass burning (8°N to 3°N; 32.9°W to 26°W), African biomass burning (3°N to 5°S; 26°W to 17°W), Southern Hemisphere (SH) marine tropics (5°S to 24.5°S; 17°W to 6.4°E), and SH marine temperate (24.5°S to 33°S; 6.4°E to 17.7°E). The meteorology resulting in these distinct regions and the chemical and physical properties of the aerosol along the cruise track are described in an overview paper in this issue [*Bates et al.*, this issue]. A figure of the cruise track, the regions, and the trajectories for each region also is included by *Bates et al.* [this issue].

Presented here are the concentrations and mass fractions of the chemical components (defined as the component concentration divided by total aerosol mass concentration), the percent of measured extinction due to each component, and mass extinction efficiencies of the chemical components for different regions. The chemical components considered include non-sea-salt

(nss) sulfate aerosol, sea salt, particulate organic matter (POM), black carbon (BC), and dust. Also presented for the regions are average aerosol scattering and absorption coefficients, the backscattered fraction, aerosol optical depth, and the portion of the aerosol optical depth due to boundary layer aerosol.

The derivation of the percent of extinction due to each component and the mass extinction efficiencies requires Mie calculations that use the measured chemical composition and number size distributions as input. To test for consistency in the input data and to assess the accuracy of the Mie calculations, closure tests were performed between measured and calculated parameters. These parameters include aerosol mass (measured gravimetrically, derived from chemical analysis, and estimated from the number size distribution) and aerosol light extinction and single scattering albedo (derived from measured light scattering and absorption coefficients and calculated from Mie theory). In addition, mass extinction efficiencies were calculated with two independent methods (Mie calculations and a multiple linear regression). Results of these comparisons are presented. A more detailed discussion of mass closure for the Aerosols99 cruise is given by S. Lienert et al. (unpublished manuscript, 2000).

2. Measurements

2.1. Aerosol Sample Inlet

Sample air for the chemical and optical measurements was drawn through a 6-m sample mast. The entrance to the mast was 18 m above sea level and forward of the ship's stack. To maintain nominally isokinetic flow and minimize the loss of supermicron particles, the inlet was rotated into the relative wind. Air entered the inlet through a 5-cm diameter hole, passed through an expansion cone, and then into the 20-cm diameter sampling mast. The flow through the mast was $1 \text{ m}^3 \text{ min}^{-1}$. The last 1.5 m of the mast were heated to establish a stable reference relative humidity (RH) for the sample air of $55 \pm 5\%$. This allows for constant instrumental size segregation in spite of variations in ambient RH, and it results in chemical, physical, and optical measurements that are directly comparable. In addition, measurement at a constant reference RH makes it possible, with the knowledge of appropriate growth factors, for end users of the data set (process, chemical transport, and radiative transfer models) to adjust the measured parameters to a desired relative humidity. All results are reported at 55% RH. Individual 1.9 cm diameter stainless steel tubes extended into the heated portion of the mast. These were connected to the aerosol instrumentation and impactors with graphite-polyethylene conductive tubing to prevent the electrostatic loss of particles. An exception to this was the lines connected to the impactors used for collection of carbonaceous aerosol; they were constructed of stainless

steel. Air was sampled only when the concentration of particles greater than 15 nm in diameter indicated the sample air was free of local contamination (i.e., there were no rapid increases in particle concentration), the relative wind speed was greater than 3 m s^{-1}, and the relative wind was forward of the beam.

2.2. Regional Concentrations of Inorganic Ions

Two-stage multijet cascade impactors [*Berner et al.*, 1979] sampling air at $55 \pm 5\%$ RH were used to determine the submicron and supermicron concentrations of Cl$^-$, NO$_3^-$, SO$_4^=$, methanesulfonate (MSA$^-$), Na$^+$, NH$_4^+$, K$^+$, Mg^{+2}, and Ca^{+2}. Sampling periods ranged from 4 to 6 hours. The RH of the sampled air stream was measured a few inches upstream from the impactor. The 50% aerodynamic cutoff diameters $D_{50,aero}$ were 1.1 and 10 μm. Throughout the paper, submicron refers to particles with $D_{aero} < 1.1$ μm at 55% RH, and supermicron refers to particles with 1.1 μm $< D_{aero} < 10$ μm at 55% RH.

The impaction stage at the inlet of the impactor was coated with silicone grease to prevent the bounce of larger particles onto the downstream stages. Tedlar films were used as the collection substrate in the impaction stage and a Millipore Fluoropore filter (1.0-μm pore size) was used for the backup filter. Films were cleaned in an ultrasonic bath in 10% H$_2$O$_2$ for 30 min, rinsed in distilled, deionized water, and dried in an NH$_3$- and SO$_2$-free glove box. Filters and films were wetted with 1 mL of spectral grade methanol. An additional 5 mLs of distilled deionized water were added to the solution and the substrates were extracted by sonicating for 30 min. The extracts were analyzed by ion chromatography [*Quinn et al.*, 1998]. All handling of the substrates was done in the glove box. Blank levels were determined by loading an impactor with substrates but not drawing any air through it.

Non-sea-salt sulfate concentrations were calculated from Na$^+$ concentrations and the ratio of sulfate to sodium in seawater. Sea-salt aerosol concentrations were calculated as

$$\text{sea salt } (\mu\text{g m}^{-3}) = \text{Cl}^- (\mu\text{g m}^{-3}) + \text{Na}^+ (\mu\text{g m}^{-3}) \times 1.47, \quad (1)$$

where 1.47 is the seawater ratio of (Na$^+$ + K$^+$ + Mg^{+2} + Ca^{+2} + SO$_4^=$ + HCO$_3^-$)/Na$^+$ [*Holland*, 1978]. This approach prevents the inclusion of non-sea-salt K$^+$, Mg^{+2}, Ca^{+2}, SO$_4^=$, and HCO$_3^-$ in the sea-salt mass and allows for the loss of Cl$^-$ mass through Cl$^-$ depletion processes. It also assumes that all measured Na$^+$ and Cl$^-$ is derived from seawater. Results of *Savoie and Prospero* [1980] indicate that dust has a minimal contribution to measured soluble sodium concentrations.

Uncertainties of the ionic chemical components at the 95% confidence level are given in Tables 1 and 2. Uncertainties were propagated as a quadratic sum of all errors involved which assumes that all errors were ran-

Table 1. Concentrations, Standard Deviations ($\pm 1\sigma$), and Absolute Uncertainties (95% Confidence Level, Shown in Parentheses) of the Mean of the Major Aerosol Submicron ($D_{aero} < 1.1$ μm at 55% RH) Chemical Species for the Different Atlantic Ocean Air Mass Regimes

Species	North America	NH Marine	Dust	Dust and Biomass Burning	Biomass Burning	SH Marine Tropics	SH Marine Temperate
nss SO$_4^=$	2.4±1.7 (0.08)	0.15±0.06 (0.004)	0.56±0.06 (0.01)	0.94±0.31 (0.02)	1.1±0.37 (0.02)	0.52±0.14 (0.008)	0.56±0.12 (0.01)
NH$_4^+$	0.54±0.34 (0.02)	0.03±0.01 (0.002)	0.09±0.01 (0.004)	0.15±0.06 (0.004)	0.19±0.07 (0.004)	0.05±0.03 (0.002)	0.04±0.005 (0.003)
MSA	0.007±0.002 (0.0002)	0.004±0.003 (0.0001)	0.008±0.002 (0.0002)	0.01±0.004 (0.0002)	0.02±0.006 (0.0003)	0.02±0.009 (0.0003)	0.04±0.01 (0.0008)
Sea salt	0.12±0.09 (0.04)	0.22±0.16 (0.02)	0.39±0.13 (0.03)	0.18±0.11 (0.05)	0.10±0.06 (0.03)	0.08±0.05 (0.03)	0.14±0.06 (0.03)
NO$_3^-$	0.04±0.03 (0.006)	0.005±0.009 (0.002)	0.05±0.03 (0.005)	0.03±0.02 (0.004)	0.01±0.01 (0.002)	<0.001	<0.001
nss sol K$^+$	0.02±0.01 (0.002)	0.002±0.002 (0.0003)	0.03±0.03 (0.001)	0.22±0.08 (0.007)	0.24±0.09 (0.007)	0.004±0.001 (0.001)	0.004±0.002 (0.001)
POM	0.78 (0.17)	0.17±0.11 (0.06)	<0.06	0.21 (0.08)	0.48±0.17 (0.11)	0.08±0.11 (0.04)	0.18±0.17 (0.1)
BC	<0.01	<0.01	0.02 (0.01)	0.30 (0.02)	0.35±0.21 (0.03)	0.01±0.03 (0.007)	<0.01
Dust/trace elements	0.02 (0.02)	0.10±0.10 (0.04)	0.73 (0.12)	0.68 (0.13)	0.09 (0.05)	0.02±0.02 (0.01)	0.02±0.02 (0.01)
Al/Si	—	0.23±0.28 (0.04)	0.33 (0.03)	0.40 (0.04)	0.32 (0.11)	0.18±0.36 (0.07)	0.38±0.66 (0.17)
Fe/Si	—	0.02±0.04 (0.004)	0.25 (0.01)	0.26 (0.02)	0.15 (0.02)	—	—

Table 2. Concentrations, Standard Deviations ($\pm 1\sigma$), and Absolute Uncertainties (95% Confidence Level, Values in Parentheses) of the Mean of the Major Aerosol Supermicron (1.1 μm < D_{aero} < 10 μm at 55% RH) Chemical Species for the Different Atlantic Ocean Air Mass Regimes

Species	Air Mass Regime, μg m^{-3}						
	North America	NH Marine	Dust	Dust and Biomass Burning	Biomass Burning	SH Marine Tropics	SH Marine Temperate
nss SO$_4^=$	0.09±0.13(0.004)	<0.001	0.03±0.10(0.003)	0.03±0.09(0.001)	0.03±0.03(0.001)	0.07±0.09(0.001)	0.03±0.04(0.001)
NH$_4^+$	<0.001	<0.001	<0.001	<0.001	<0.001	<0.001	<0.001
MSA	0.001±0.003(0.0001)	0.005±0.004(0.0001)	0.006±0.004(0.0002)	0.009±0.008(0.0002)	0.007±0.006(0.0001)	0.03±0.018(0.0005)	0.06±0.02(0.001)
Sea salt	9.2±4.6(0.3)	8.0±2.8(0.12)	19±2.9(0.46)	8.2±4.9(0.23)	4.6±2.6(0.09)	6.4±3.2(0.1)	9.5±2.8(0.18)
NO$_3^-$	2.30±1.6(0.08)	0.23±0.23(0.008)	0.76±0.25(0.02)	1.3±0.55(0.02)	0.94±0.55(0.02)	0.19±0.11(0.007)	0.14±0.06(0.01)
nss sol K$^+$	<0.001	0.008±0.03(0.0004)	0.002±0.002(0.0001)	0.01±0.01(0.0003)	0.02±0.01(0.0003)	0.004±0.003(0.0001)	0.001±0.001(0.0001)
POM	0.67(0.16)	0.38±0.09(0.07)	1.0(0.16)	0.73(0.14)	0.32±0.27(0.2)	0.28±0.18(0.07)	0.23±0.11(0.11)
BC	<0.01	<0.01	0.01(0.01)	0.06(0.02)	<0.03	<0.01	<0.01
Dust/trace elements	0.57(0.43)	0.26±0.34(0.05)	21(3)	24(3.6)	1.9(0.34)	0.17±0.21(0.05)	0.06±0.03(0.04)
Al/Si	—	0.31±0.43(0.03)	0.32(0.02)	0.34(0.02)	0.30(0.02)	0.57±0.69(0.39)	—
Fe/Si	—	0.07±0.16(0.005)	0.24(0.01)	0.24(0.01)	0.26(0.02)	0.12±0.20(0.01)	—

dom. Details of the uncertainty analysis are given by *Quinn et al.* [2000].

2.3. Regional Concentrations of Total Organic and Black Carbon

Three-stage multijet cascade impactors [*Berner et al.*, 1979] sampling air at 55 ± 5% RH were used to determine submicron and supermicron concentrations of total, organic, and black carbon. The impactor had $D_{50,aero}$ of 0.18, 1.1, and 10 μm. Only in this case does submicron refer to 0.18 < D_{aero} < 1.1 μm. The 0.18 μm jet plate was used instead of a quartz backup filter to minimize positive artifacts due to the absorption of gas phase organics. Sampling periods ranged from 12 to 24 hours. Al foils, used as sampling substrates, were heated at the Institute for Tropospheric Chemistry (Leipzig, Germany) before the cruise at 600°C for 4 hours to remove organic contaminants. Blank levels were determined by placing substrates into a second impactor and deploying the impactor for the duration of the sampling period without drawing air through it. Foils were stored frozen until analysis.

The samples were analyzed by a thermographic method using a commercial instrument (C-mat 5500, Ströhlein) [*Neusüss et al.*, 2000]. The sample is placed in a quartz tube and heated rapidly to a specific temperature. To separate organic carbon (OC) and BC, the sample is first heated to 590°C under nitrogen. The carbon compounds that evaporate under these conditions are referred to as OC. Then the sample is heated under oxygen to 650°C, and all carbon except carbonate is oxidized. The evaporated carbon is completely oxidized to CO_2 followed by analysis with an IR detector. External standards are used to calibrate the measurements. As with all thermal carbon measurements, the OC/BC split is a method dependent property.

The mass of particulate organic matter (POM) was determined by multiplying the measured organic carbon concentration in μg C m^{-3} by a POM factor which is an estimated average of the molecular weight per carbon weight for the organic aerosol. On the basis of a review of published measurements of the composition of organic aerosol in urban and non-urban regions, *Turpin and Lim* [2000] found that values of 1.6 ± 0.2 and 2.1 ± 0.2 most accurately represent urban and non-urban aerosols, respectively. A value of 1.6 was used for the North American air masses, and a value of 2.1 was used for all other air mass regions. The POM factor was assigned an absolute uncertainty of 0.35.

The uncertainties associated with positive and negative sampling artifacts can be substantial [*Turpin et al.*, 1994, 2000]. An effort was made to minimize positive artifacts by collecting samples on impaction plates. Negative artifacts may have occurred as a result of the pressure drop across the impactor (9 mbar for the 1.1 μm jet plate and 530 mbar for the 0.18 μm jet plate). No attempt was made to correct for artifacts or to determine

their associated uncertainties since the information to do so was not available.

Uncertainties of the POM and BC concentrations at the 95% confidence level are reported in Tables 1 and 2. The uncertainties for BC are based on 2 times the standard deviation of the blank values measured over the course of the experiment. The uncertainties for POM are based on a quadrature sum of the uncertainty in the OC to POM conversion factor and 2 times the standard deviation of the blank over the course of the experiment.

2.4. Regional Concentrations of Dust and Trace Elements

Total elemental composition (Na, Mg, Al, Si, P, Cl, K, Ca, Ti, V, Cr, Mn, Fe, Ni, Cu, Zn, Ba, As, and Pb) was determined by thin-film X-ray primary- and secondary-emission spectrometry [Feely et al., 1991, 1998]. Submicron samples were collected on Nuclepore filters (0.4 μm pore size) mounted in a Berner impactor downstream of the $D_{50,aero}$ 1.1 μm jet plate. Bulk samples were collected on Nuclepore filters (0.4 μm pore size) in a filter pack having an upper $D_{50,aero}$ of 10 μm. Supermicron elemental concentrations were determined by difference between the submicron and bulk samples. This method of sample collection allows for the sharp size cut of the impactor while collecting a thin film of aerosol necessary for the X-ray analysis. Sampling periods ranged from 12 to 24 hours.

Filters were acid washed before sample collection by soaking in 4 N HNO_3 for 24 hours and then 2% HCl for 24 hours with multiple rinses with distilled deionized water between treatments. Filters were weighed before and after sample collection as described below. Blank levels were determined by loading an impactor or filter pack with a filter but not drawing any air through it.

For the regions of African dust and the dust/biomass burning mixture, dust concentrations were calculated from the Al mass concentration and an assumed dust to Al mass ratio of 12.5. This is based on the relatively constant 8% mass fraction of Al found in continental soils including Saharan dust (D. Savoie, personal communication, 2000). An uncertainty of ±20% was attached to the factor of 12.5. Outside of these regions the concentrations of all elements measured by XRF were summed to create a "trace element" component mass concentration. Since the molecular form of the elements was not determined, the summed concentrations do not include any associated mass (e.g., the oxygen associated with aluminum oxide). This does not have a large effect on the overall mass closure, however, as the trace elements were a minor component of the mass (0.05 to 9% for the submicron mass and 0.2 to 1.9% for the supermicron mass) outside of the dust-containing regions. If the dominant elements in most regions (Al, Si, and Fe) were in their oxide form, the mass would have been underestimated by about 75%. Hence an error of 75% was included in the uncertainty calculations.

Uncertainties at the 95% confidence level associated with the major elemental species (Al, Si, and Fe) are reported in Tables 1 and 2. Uncertainties were propagated as a quadratic sum of all errors involved including those due to the X-ray analysis, blank approximation, and volume of air sampled. XRF analysis errors are based on 2 times the standard deviation of 15 replicate analyses of a sample filter. Blank errors are based on 2 times the standard deviation of the average of all blanks collected over the course of the experiment.

2.5. Regional Mass Fractions

Submicron and supermicron regional mass fractions were calculated from concentrations of the measured chemical components and the XRF Nuclepore filters that were weighed before and after sample collection. The filters were weighed at PMEL with a Cahn Model 29 microbalance housed in a glove box kept at a humidity of 33 ± 2%. The resulting mass concentrations from the gravimetric analysis include the water mass that is associated with the aerosol at 33% RH. Additional water mass may also be present due to interactions between the collected aerosol and the sampling substrate. The response of particles collected on a filter to changes in RH has been shown to be different than that of individual particles or bulk solutions of similar chemical composition [McInnes et al., 1996].

The glove box was continually purged with room air that had passed through a scrubber of activated charcoal, potassium carbonate, and citric acid to remove gas phase organics, acids, and ammonia. Static charging, which can result in balance instabilities, was minimized by coating the walls of the glove box with a static dissipative polymer (Tech Spray, Inc.), placing an antistatic mat on the glove box floor, using antistatic gloves while handling the substrates, and exposing the substrates to a ^{210}Po source to dissipate any charge that had built up on the substrates. Before and after sample collection, substrates were stored double-bagged with the outer bag containing citric acid to prevent absorption of gas phase ammonia. More details of the weighing procedure are given by Quinn and Coffman [1998].

Uncertainties of the mass fractions at the 95% confidence level are shown in Figures 3 and 4 and are based on a quadratic sum of the uncertainties of the chemical concentrations and the gravimetrically determined mass. Uncertainty in the latter includes errors due to weighing, storage and transport, and the volume of air sampled [Quinn et al., 2000]. To maintain the sampling RH of 55%, the sample air was heated, on average, 5.4°C (range of heating was 2° to 10°C). This heating may have led to the volatilization of a portion of the semivolatile organics and ammonium nitrate from the substrate [Ayers et al., 1999] thereby resulting in artificially low masses. No attempt was made to correct for the artifact, however, as the composition of the semivolatile organics was unknown.

2.6. Aerosol Scattering, Backscattering, and Absorption Coefficients

Measurements of aerosol scattering and hemispheric backscattering coefficients were made with an integrating nephelometer (Model 3563, TSI Inc.) at wavelengths of 450, 550, and 700 nm at 55% RH. The RH was measured inside the nephelometer sensing volume. A single-stage impactor with a $D_{50,aero}$ of 10 μm was placed upstream of the nephelometer. Values measured directly by the nephelometer were corrected for an offset determined by measuring filtered air over a period of several hours [*Anderson and Ogren*, 1998]. In addition, they were corrected for the angular non idealities (including truncation errors and nonlambertian response) of the nephelometer using

$$\sigma_{sp} = \sigma_{sp\_Meas} \times \frac{\sigma_{sp\_True}}{\sigma_{sp\_Neph\_sim}}, \qquad (2)$$

where σ_{sp_True} is the "true" scattering coefficient determined from the measured number size distribution and chemistry and a Mie scattering model and $\sigma_{sp\_Neph\_sim}$ is the nephelometer simulated scattering coefficient determined from a Mie scattering model which employs a Mie integral modified to simulate the nephelometer response [*Quinn and Coffman*, 1998]. (The Mie calculations are discussed in more detail below.) This correction is similar to that of *Anderson and Ogren* [1998] but uses the simultaneously measured size distribution rather than an assumed size distribution. Values are reported at 0°C and 1013 mbar.

Sources of uncertainties associated with the use of the integrating nephelometer include photon counting during measurement, zeroing, and calibration; literature values of calibration gas scattering coefficients; variations in gas density within the nephelometer, and the angular correction applied in equation (2). These uncertainties were estimated using the method of *Anderson et al.* [1999]. Additional uncertainties include variations in measured scattering due to RH changes within the nephelometer sensing volume and inlet losses of large particles [*Quinn and Coffman*, 1998]. For a 30-min averaging time a quadrature sum of errors yielded absolute uncertainties of 4.1 and 20 Mm^{-1} corresponding to low and high values of σ_{sp} equal to 24 and 110 Mm^{-1}, respectively. Absolute uncertainties for σ_{bsp} equal to 3.0 and 13 Mm^{-1} were 0.32 and 1.3 Mm^{-1}, respectively.

The absorption coefficient for sub-10 μm aerosol, σ_{ap}, was measured at 55% RH by monitoring the change in transmission through a filter with a Particle Soot Absorption Photometer (PSAP, Radiance Research). Measured values were corrected for a scattering artifact, the deposit spot size, the PSAP flow rate, and the manufacturer's calibration as per *Bond et al.* [1999]. Values are reported at 0°C, 1013 mbar, and 550 nm. Sources of uncertainty in the PSAP measurement include noise, drift, correction for the manufacturer's calibration, and correction for the scattering artifact [*Anderson et al.*, 1999]. A quadrature sum of these errors yields absolute

uncertainties of 0.38 and 2.8 Mm^{-1} for σ_{ap} equal to 0.68 and 13 Mm^{-1}, respectively, for a 30-min averaging time.

2.7. Number Size Distribution

Size distributions from 5 nm to 5 μm were measured with the combination of an ultrafine differential mobility particle sizer (UDMPS, University of Vienna (Reischle) short column), a differential mobility particle sizer (DMPS, University of Vienna (Reischle) medium column), and an aerodynamic particle sizer (APS) (TSI 3300) [*Bates et al.*, this issue]. The UDMPS and DMPS were operated at 55 ± 5% RH. The APS was operated dry. Diameters were shifted to 55% RH using the mass of water calculated to be associated with the aerosol at that RH (see section 3.1 for details of water calculation). Filtered mobility distributions from the DMPSs were converted to number size distributions using the inversion routine of *Stratman and Wiedensohler* [1997]. Data were corrected for diffusional losses [*Covert et al.*, 1997] and size-dependent counting efficiencies [*Wiedensohler et al.*, 1997]. DMPS diameters were converted to aerodynamic diameters by multiplying by the square root of the particle density determined from the size-resolved chemical measurements. An interactive routine was used to fit lognormal curves to the different modes of the number size distribution [*Quinn and Coffman*, 1998].

Uncertainties in the measured number size distribution (and mass concentrations derived from the number size distribution) result from instrumental errors of particle sizing and counting due to flow instabilities in the DMPS and APS. The amount of observed drift in the sheath and excess flows led to a ±20% uncertainty in the number concentration [*Bates et al.*, this issue]. Additional factors affecting the accuracy of the conversion of the number concentration to a mass concentration include errors in the measured chemical composition and calculated density. Overall uncertainties in the submicron mass concentration derived from the number size distribution are ±35% for a concentration of 3 μg m^{-3} [*Quinn and Coffman*, 1998]. Uncertainties for supermicron mass concentrations are ±25% for a concentration of 20 μg m^{-3}.

2.8. Aerosol Optical Depth

Aerosol optical depths reported here are based on an averaging of values from several instruments including three handheld sunphotometers (Microtops, Solar Light Co.), a Simbad radiometer, a fast rotating shadowband radiometer (FRSR) [*Reynolds et al.*, 2001], and a micropulse lidar [*Spinhirne et al.*, 1995] (E. J. Welton et al., Aerosol and cloud measurements using micropulse lidar systems, submitted to *Journal of Atmospheric and Oceanic Technology*, 2000, hereinafter referred to as Welton et al., submitted manuscript, 2000). Ångström exponents based on the optical depth values were derived from all of the above instruments except

the lidar. Average aerosol optical depths and Ångström exponents were calculated for all of the cruise at $\frac{1}{4}$ day intervals [*Voss et al.*, this issue (a)] from the various instruments. A third order polynomial was fit to 1.5 days of data centered on the desired time. This polynomial was then used to interpolate the τ_a for the desired $\frac{1}{4}$ day interval in increments of 1/200 day. To determine the degree of variability in the different instruments, three time periods when the τ_a was stable throughout the day were considered. Average τ_a and 1σ standard deviations were 0.31 ± 0.03, 0.13 ± 0.02, and 0.1 ± 0.02 for the three time periods. Hence, τ_a derived from the different instruments varied between 9 and 20% with greater variations for lower τ_a. More details about the compilation of τ_a data, measurement uncertainties, and discrete measurements obtained in each region are given by *Voss et al.* [this issue (a)].

2.9. Ancillary Parameters

Also measured were meteorological parameters including surface temperature, RH, wind speed and direction, as well as vertical profiles of these parameters from radiosondes. Air mass back trajectories were calculated for three arrival altitudes (500, 2500, and 5500 m) for the ship's position at 6-hour intervals. Trajectories were calculated with the hybrid single-particle Lagrangian integrated model HY-SPLIT 4 based on the FNL global wind field [*Draxler*, 1992] (http://www.noaa.gov/ready-bin/fnl.pl).

3. Model Calculations

3.1. Calculation of Aerosol Water Mass, Density, and Refractive Index

The gravimetric analysis was performed at 33% RH. Hence the measured mass on the filter substrates included the amount of water associated with the aerosol at that RH. The impactors, nephelometer, and PSAP sampled aerosol at 55% RH. The chemical thermodynamic equilibrium model AeRho [*Quinn et al.*, 1998; *Quinn and Coffman*, 1998] was used to estimate the water mass associated with the inorganic ions at 33 and 55% RH so that the gravimetric and chemically analyzed mass could be adjusted to the RH of the optical measurements. No information was available on the chemical composition or hygroscopicity of the organic mass. Therefore no attempt was made to calculate its associated water mass. Likewise, the trace element components estimated from the XRF analysis were assumed to be hygrophobic.

Using the aerosol chemical composition measured with seven-stage multijet cascade impactors [*Berner et al.*, 1979] ($D_{50,aero}$ of 0.18, 0.31, 0.55, 1.1, 2.0, 4.1, and 10 μm), AeRho also was used to calculate the refractive index and density of the mix of all aerosol components (for the calculation of total extinction) and for the individual chemical components (for the calculation

Table 3. Chemical Reactions Included in the Chemical Equilibrium Model AeRho

Reaction	Crystallization RH
$2H^+_{(aq)} + SO_4^=_{(aq)} \leftrightarrow H_2SO_{4(aq)}$	
$H^+_{(aq)} + HSO_4^-_{(aq)} \leftrightarrow H_2SO_{4(aq)}$	
$2NH_4^+_{(aq)} + SO_4^=_{(aq)} \leftrightarrow (NH_4)_2SO_{4(aq)}$	
$NH_4^+_{(aq)} + HSO_4^-_{(aq)} \leftrightarrow NH_4HSO_{4(aq)}$	
$2Na^+_{(aq)} + SO_4^=_{(aq)} \leftrightarrow Na_2SO_{4(aq)}$	
$Na^+_{(aq)} + HSO_4^-_{(aq)} \leftrightarrow NaHSO_{4(aq)}$	
$2K^+_{(aq)} + SO_4^=_{(aq)} \leftrightarrow K_2SO_{4(aq)}$	
$K^+_{(aq)} + HSO_4^-_{(aq)} \leftrightarrow KHSO_{4(aq)}$	
$H^+_{(aq)} + NO_3^-_{(aq)} \leftrightarrow HNO_{3(aq)}$	
$NH_4^+_{(aq)} + NO_3^-_{(aq)} \leftrightarrow NH_4NO_{3(aq)}$	
$Na^+_{(aq)} + NO_3^-_{(aq)} \leftrightarrow NaNO_{3(aq)}$	
$K^+_{(aq)} + NO_3^-_{(aq)} \leftrightarrow KNO_{3(aq)}$	
$H^+_{(aq)} + Cl^-_{(aq)} \leftrightarrow HCl_{(aq)}$	
$NH_4^+_{(aq)} + Cl^-_{(aq)} \leftrightarrow NH_4Cl_{(aq)}$	
$Na^+_{(aq)} + Cl^-_{(aq)} \leftrightarrow NaCl_{(aq)}$	
$K^+_{(aq)} + Cl^+_{(aq)} \leftrightarrow KCl_{(aq)}$	
$2NH_4^+_{(aq)} + SO_4^=_{(aq)} \leftrightarrow (NH_4)_2SO_{4(s)}$	40[a]
$NH_4^+_{(aq)} + HSO_4^-_{(aq)} \leftrightarrow NH_4HSO_{4(s)}$	22[a]
$2Na^+_{(aq)} + SO_4^=_{(aq)} \leftrightarrow Na_2SO_{4(s)}$	59[a]
$Na^+_{(aq)} + HSO_4^-_{(aq)} \leftrightarrow NaHSO_{4(s)}$	0.05[b]
$2K^+_{(aq)} + SO_4^=_{(aq)} \leftrightarrow K_2SO_{4(s)}$	62[c]
$K^+_{(aq)} + HSO_4^-_{(aq)} \leftrightarrow KHSO_{4(s)}$	62[c]
$NH_4^+_{(aq)} + NO_3^-_{(aq)} \leftrightarrow NH_4NO_{3(s)}$	32[b]
$Na^+_{(aq)} + NO_3^-_{(aq)} \leftrightarrow NaNO_{3(s)}$	30[b]
$K^+_{(aq)} + NO_3^-_{(aq)} \leftrightarrow KNO_{3(s)}$	62[c]
$NH_4^+_{(aq)} + Cl^-_{(aq)} \leftrightarrow NH_4Cl_{(s)}$	47[d]
$Na^+_{(aq)} + Cl^-_{(aq)} \leftrightarrow NaCl_{(s)}$	45[e]
$K^+_{(aq)} + Cl^-_{(aq)} \leftrightarrow KCl_{(s)}$	62[e]

[a] *Tang and Munkelwitz* [1994].
[b] *Tang* [1996].
[c] No data, assumed from KCl.
[d] *Cohen et al.* [1987].
[e] *Tang et al.* [1997].

of extinction fractions and mass extinction efficiencies). Details of the AeRho calculations are given below.

For the purpose of reconciling all the various in situ measurements, AeRho is a static model. It is designed to take the measured ionic composition of the aerosol and the constant sampling RH and to determine the molecular composition of the ionic chemical species within the aerosol. The molecular composition then is used to calculate the water mass associated with the aerosol and the aerosol refractive index and density. The model is not used to describe a dynamic system in which changes in the concentration of gas phase species affect the aerosol molecular composition. Therefore the model does not include interactions between the gas and aqueous phases. In addition, because of the constant sampling RH, it is not necessary to take into account changes in particle size with changes in RH.

For the calculation of total extinction, the aerosol was assumed to be an internal mixture containing all measured chemical components. The chemical reactions allowed to occur are shown in Table 3. The ionic molalities for each of the input species are determined initially by assuming that the activity of water is equal to the instrumental RH. Then, using the ZSR method [Zdanovskii, 1936; Robinson and Stokes, 1965], a further approximation of the water content of the aerosol is made. Aqueous phase concentrations are activity corrected using the method of Bromley [1973] which allows for the prediction of activity coefficients of strong electrolytes in multielectrolyte solutions based on binary solution activity coefficients [Pilinis and Seinfeld, 1987]. The pure-solution binary activity coefficients are calculated using the method of Pitzer and Mayorga [1973]. The ionic species are partitioned between the solid and aqueous phases with the solids precipitating in the most thermodynamically favorable order. The crystallization RH used for each solid phase species is listed in Table 3. The remaining aqueous ionic species are converted to aqueous compounds in accordance with the thermodynamic equilibrium constants. Finally, thermodynamic equilibrium with respect to water is tested for, and the water activity is iterated until equilibrium is established.

Polynomial fits based on data of Tang and Munkelwitz [1991, 1994] for metastable particles are used to estimate densities of individual inorganic soluble species. Data from Bray [1970] are used to estimate the density of H_2SO_4. The density of OC was assumed to be 1.4 g cm^{-3} [Turpin and Lim, 2000], and that of BC was assumed to be 2 g cm^{-3} [Seinfeld and Pandis, 1998]. The density of dust in the African dust and dust/biomass burning air mass regions was set equal to that of illite (2.75 g cm^{-3}) as illite is a major component of African dust [Sokolik and Toon, 1999]. In the regions not influenced by dust from Africa, the trace element component was assumed to have a density of 2.3 g cm^{-3}.

A volume-weighted average was taken of the density of the individual species to estimate the density of the aerosol mix in each impactor size bin. Average submicron and supermicron densities for each region for the mix of aerosol chemical components are reported in Table 4.

The method of partial molar refractions [Stelson, 1990] was used to calculate the real portion of the refractive index as a function of size. Values of the partial molar refractions of all chemical species except dust were taken from Stelson [1990]. The complex refractive index was obtained by volume averaging the refractive index of the scattering and absorbing components. The refractive index used for African dust was $1.56-0.001i$ based on measurements of Saharan dust [Patterson et al., 1977]. The refractive index used for the trace element component was $1.53-0.005i$. Average submicron and supermicron refractive indices for each region for the mix of aerosol chemical components are reported in Table 4.

For the calculation of the extinction due to each chemical component and mass extinction efficiencies, the method described above was followed, but only individual components were considered. For components containing more than one chemical species (e.g., $H_2SO_4/NH_4HSO_4/(NH_4)_2SO_4$ in the nss sulfate aerosol), a volume-weighted average was taken of the density of the individual species to estimate the density of the component in each impactor size bin. Similarly, the method of partial molar refractions was used to calculate the real portion of the refractive index as a function of size for the water-soluble chemical components containing more than one chemical species.

3.2. Calculation of Extinction Due to Each Chemical Component and Mass Extinction Efficiencies

The chemical components considered in this analysis are sea salt, nss sulfate, dust, POM, and BC. The sea-

Table 4. Regional Averages of Submicron ($D_{aero} < 1.1$ μm) and Supermicron ($1.1 < D_{aero} < 10$ μm) Densities and Real and Imaginary Portions of the Refractive Index Estimated From the Chemical Thermodynamic Equilibrium Model, AeRho[a]

Region	Density, g cm^{-3}		Refractive Index Real Portion		Refractive Index Imaginary Portion	
	Sub-μm	Super-μm	Sub-μm	Super-μm	Sub-μm	Super-μm
North America	1.47	1.26	1.51	1.42	2.3E-05[b]	5.9E-05
NH marine	1.37	1.30	1.45	1.44	6.3E-05	1.9E-05
African dust	1.85	1.70	1.54	1.47	3.9E-03	4.0E-04
African dust/biomass burning	2.11	1.94	1.66	1.49	7.0E-02	1.1E-03
Biomass burning	1.91	1.56	1.69	1.46	5.8E-02	1.9E-04
SH marine tropics	1.67	1.32	1.57	1.44	5.4E-05	2.7E-05
SH marine temperate	1.76	1.30	1.58	1.44	1.8E-04	1.0E-05

[a] Values are reported for 55% RH.

[b] Read 2.3E-05 as 2.3×10^{-5}.

salt component includes all measured NO_3^- in the supermicron size range on the assumption that gas phase HNO_3 resulting from combustion processes reacts with sea salt to form $NaNO_3$ [*Clegg and Brimblecombe*, 1985]. NSS sulfate aerosol includes nss $SO_4^=$ and all measured NH_4^+ up to an NH_4^+ to nss $SO_4^=$ molar ratio of 2. The sea salt and nss sulfate components also include the water calculated to be associated with these components at 55% RH. A combustion component composed of BC and submicron soluble nss K^+, nss $SO_4^=$, and NO_3^- was constructed whose refractive index and density were determined by mass averaging those of the individual species. The submicron nss $SO_4^=$ added to the combustion component was found by the equilibrium calculation to be in excess of an NH_4^+ to nss $SO_4^=$ molar ratio of 2. NO_3^- and nss $SO_4^=$, assumed here to be in the form of KNO_3 and K_2SO_4, have been measured in biomass burning plumes by *Liu et al.* [2000].

Size distributions of sea salt and nss sulfate aerosol were determined from the seven-stage impactor measurements coupled with the number size distributions (see below). Since only submicron and supermicron samples were collected for the remaining components, it was necessary to assume their size distributions. POM and the combustion component were distributed as nss sulfate aerosol. The dust and summed trace element components were distributed as sea salt. As discussed below in section 4.3.4, mass extinction efficiencies derived with the Mie calculational method described here compare well with those derived from an independent empirical multiple linear regression method. In addition, the values are within the range of those previously reported, indicating that the size distribution assumptions were reasonable.

Using the output from AeRho, a volume ratio (component volume/total aerosol volume) was calculated for each component within each impactor size bin from the component mass concentration and density (both determined from AeRho) in the size bin. Component surface area ratios were then derived from the volume ratios.

Extinction coefficients (σ_{ep}, Mm^{-1}) were calculated for each component using the total aerosol surface area fit parameters (from the measured number size distributions) and the component surface area ratios. Surface area fit parameters based on the number size distribution measured at $55 \pm 5\%$ RH are given in Table 5. This approach uses the measured chemical information but maintains the higher size resolution of the measured number size distribution. (It also requires agreement between the mass derived from the impactors and the mass derived from the number size distribution. As discussed in section 4.1, for the submicron size range these independent measures of mass agreed within the overall experimental uncertainty for all regions except the SH marine tropics. For the supermicron size range they agreed within the experimental uncertainty for all regions.) Having acquired size distributions of σ_{ep} for each component, values of submicron and supermicron component σ_{ep} were determined by integrating over the appropriate size range. Mass extinction efficiencies (m^2 g^{-1}) were calculated from the component $\sigma_{ep,j}$ (Mm^{-1}) and mass concentrations (μg m^{-3}) for the submicron, supermicron, and $D_{aero} < 10$ μm size ranges.

4. Results

4.1. Comparison of Measured and Calculated Aerosol Mass and Extinction

Mean regional values of three measures of mass were compared to assess internal consistency in the impactor and number size distribution data used in the extinction calculations. A more detailed description of mass closure for the cruise which goes beyond regional averages is presented in S. Leinert et al. (unpublished manuscript, 2000). Submicron and supermicron aerosol mass concentrations were determined gravimetrically, by summing the chemically analyzed species, and from the number size distribution using the density of the total aerosol mixture estimated with AeRho. The amount of water calculated to be associated with the aerosol at

Table 5. Accumulation and Coarse Mode Surface Area Fit Parameters (Mean Values and 1σ Standard Deviation) at 55% RH

Region	Accumulation Mode			Coarse Mode 1[a]			Coarse Mode 2		
	S, μm cm^{-3}	D_{gs}, μm	σ_g	S, μm cm^{-3}	D_{gs}, μm	σ_g	S, μm cm^{-3}	D_{gs}, μm	σ_g
North America	84 ± 23	0.25 ± 0.01	1.4 ± 0.03	39 ± 20	0.8 ± 0.07	1.8 ± 0.48	48 ± 14	$2.8 + 0.19$	$1.6 + 0.11$
NH marine	8 ± 2	0.22 ± 0.03	1.4 ± 0.11	28 ± 12	1.2 ± 0.35	2.1 ± 0.52	47 ± 17	$2.7 + 0.28$	$1.7 + 0.15$
African dust	11 ± 2	0.18 ± 0.01	1.4 ± 0.03	50 ± 16	0.9 ± 0.16	1.9 ± 0.22	82 ± 17	$2.1 + 0.11$	$1.6 + 0.06$
African dust/BB	52 ± 9	0.27 ± 0.01	1.7 ± 0.08	78 ± 17	1.7 ± 0.04	1.7 ± 0.02			
Biomass burning	52 ± 13	0.27 ± 0.01	1.5 ± 0.03	17 ± 6	1.8 ± 0.09	1.7 ± 0.06			
SH marine tropical	19 ± 6	0.3 ± 0.02	1.5 ± 0.07	27 ± 10	2.1 ± 0.08	1.9 ± 0.07			
SH marine temperate	24 ± 4	0.25 ± 0.01	1.3 ± 0.03	53 ± 7	2.4 ± 0.11	2.1 ± 0.13			

[a]The coarse aerosol was fit with two lognormal modes in the North America, NH marine, and dust regions to accommodate a bimodal structure. The two-mode fit results in the best representation of both the total surface area concentration and the mean diameter of the coarse aerosol [*Quinn and Coffman*, 1998].
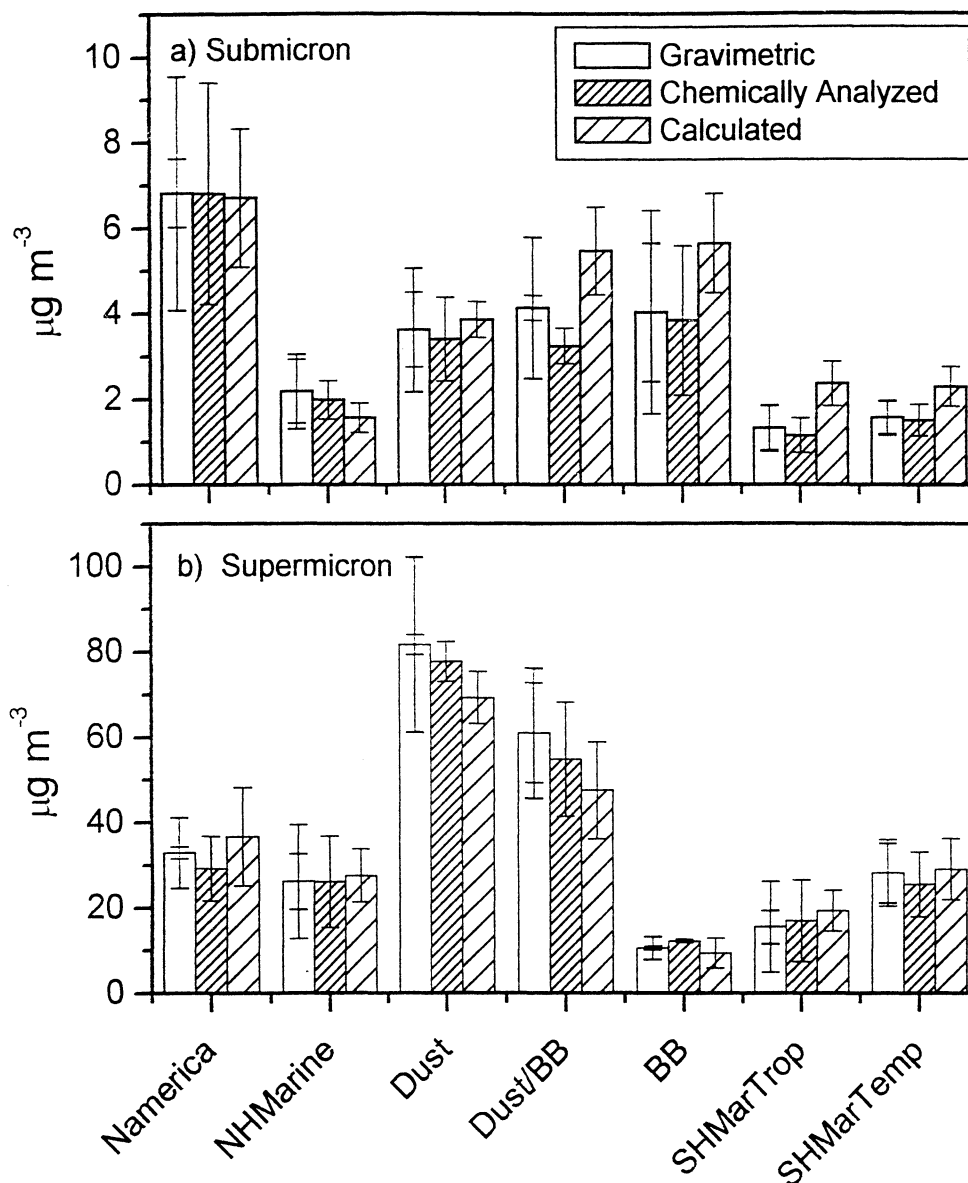
Figure 1. Comparison of three measures of the aerosol mass concentration at 55% RH for the (a) submicron and (b) supermicron size ranges. Gravimetric denotes the gravimetrically analyzed mass; chemically analyzed is the sum of the mass analyzed for inorganic ions, organic and black carbon, and trace elements. Both the gravimetric and chemically analyzed mass include the water calculated to be associated with the inorganic ions at 55% RH. Calculated denotes the mass estimated from the number size distribution and the density based on the measured chemical composition. Black error bars indicate the 1σ standard deviation of the mean. Gray error bars indicate the overall uncertainty for the mass closure experiment.

55% RH was added to the gravimetric and chemically analyzed mass to adjust them to the measurement RH of the number size distribution. As shown in Figure 1, submicron mass concentrations from the three methods agreed within the overall uncertainty of the closure experiment for all regions except the SH marine tropics. (Overall uncertainty was calculated from a quadrature sum of the uncertainties from each of the three methods [*Quinn and Coffman*, 1998].) The number-derived submicron mass concentration for the SH marine tropics was, on average, a factor of 2 higher than the sum

of the chemically analyzed mass. This discrepancy will result in an overestimation of the submicron extinction coefficient for each component. Supermicron mass concentrations from the three methods agreed within the overall experimental uncertainty for all regions. The agreement within experimental uncertainty for all regions except the SH marine tropics indicates that closure was obtained and that the chemical analysis accounted for all of the species that were present in the aerosol.

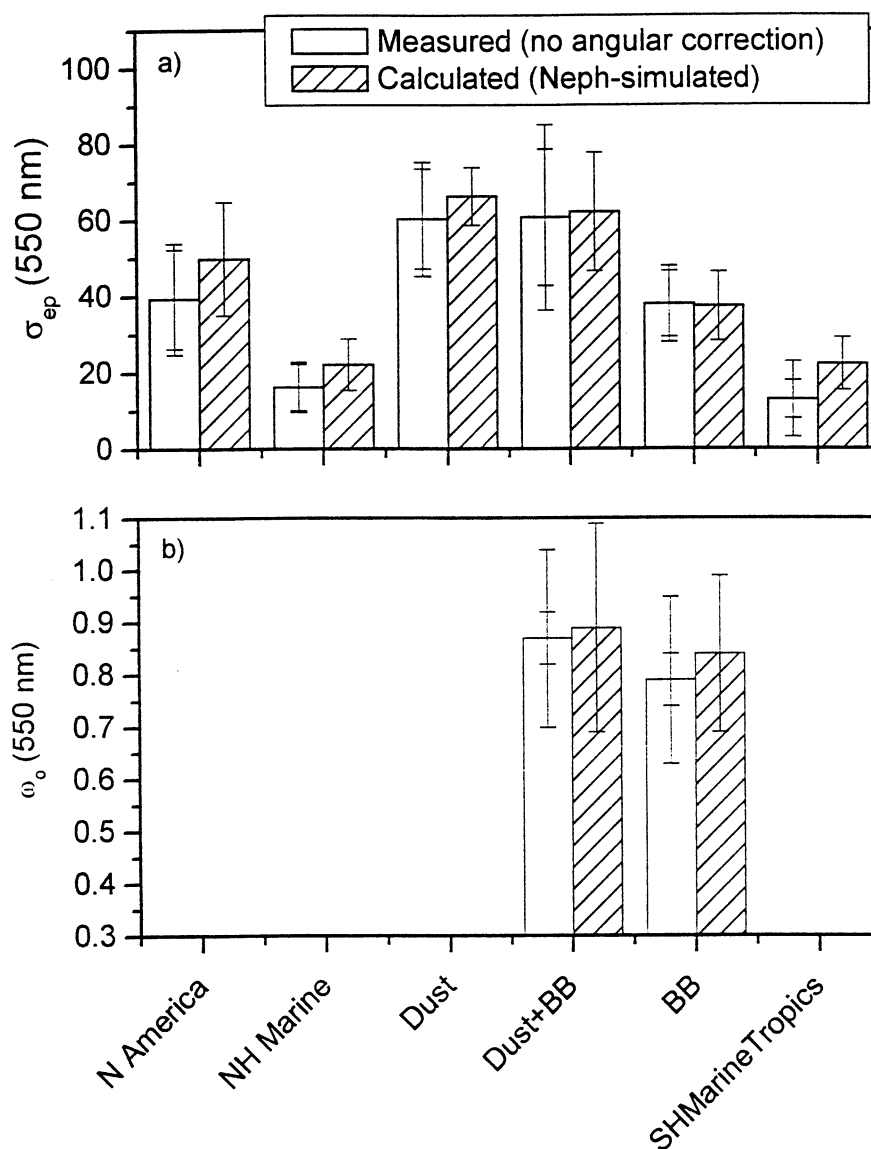Extinction for particles with $D_{\text{aero}} < 10$ μm was de-

Figure 2. (a) Comparison of the mean measured extinction (sum of the STP-corrected σ_{sp} from the nephelometer and σ_{ap} from the PSAP) and the calculated extinction (sum of the nephelometer-simulated σ_{sp} and σ_{ap}) for $D_{aero} < 10$ μm for each air mass region. (b) Comparison of the measured and calculated single scattering albedo for two of the air mass regions. Black error bars indicate the 1σ standard deviation of the mean. Gray error bars indicate the overall uncertainty for the mass closure experiment.

rived from the measured scattering and absorption coefficients. In addition, extinction for the same size range was estimated using the measured chemical composition and number size distributions as input to Mie calculations. Measured and calculated extinction agreed within the overall uncertainty of the closure experiment for all regions except the SH marine tropics (Figure 2). Since submicron mass closure and extinction closure was not obtained for the SH marine tropics, extinction fractions and mass extinction efficiencies were not calculated for this region. In addition, due to instrument malfunction, scattering coefficients were not measured in the SH marine temperate region making it impossible to compare measured and calculated extinction. There-

fore extinction fractions and mass extinction efficiencies were not calculated for this region.

As an additional check on the extinction calculations, measured and calculated single scattering albedos were compared for the dust/biomass burning and biomass burning regions, the two regions in which measured absorption coefficients were above the detection limit. As shown in Figure 2, agreement was within the overall experimental uncertainty for both regions.

4.2. Regional Chemical Composition and Mass Fractions

4.2.1. Sulfate aerosol. Table 1 lists the concentrations, standard deviations, and absolute uncer-
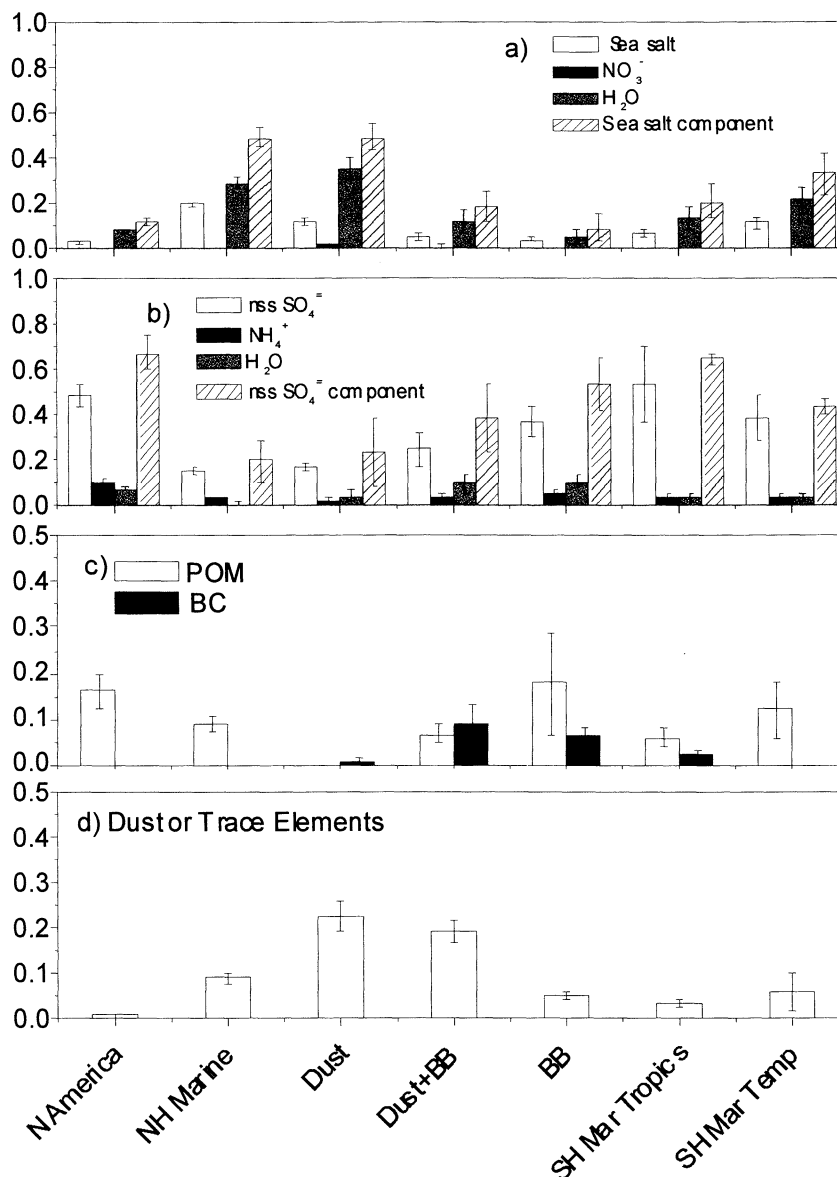
Figure 3. Mean submicron ($D_{50,\text{aero}} < 1.1$ μm at 55% RH) mass fractions of the dominant chemical components for the seven air mass regions. Error bars indicate the uncertainty in the mean mass fraction for each region at the 95% confidence level. The sea-salt component mass includes sea salt, nitrate, and water. The nss sulfate component includes nss $SO_4^=$, NH_4^+, and water. The number of samples available for the mass fraction calculation in each region was as follows: North America, 1; NH marine, 4; dust, 2; Dust plus biomass burning (BB), 2; BB, 2; SH marine tropics, 6; SH marine temperate, 3.

tainties of the mean of the major submicron aerosol chemical species for the different air mass regions. Submicron nss $SO_4^=$ and NH_4^+ concentrations were highest in the North America air mass (mean and standard deviation (1σ) of 2.4 $\pm$ 1.7 μg m^{-3} and 0.54 $\pm$ 0.34, respectively). These concentrations are similar to those measured in polluted air masses advected from North America to Sable Island, Nova Scotia (nss $SO_4^=$ of 2.7 μg m^{-3}) [*Quinn et al.*, 2000]. Mean concentrations in the biomass burning air mass region (nss $SO_4^=$ = 1.1 $\pm$ 0.37 and NH_4^+ = 0.19 $\pm$ 0.07) were slightly higher than

in the dust/biomass burning mixture (nss $SO_4^=$ = 0.94 $\pm$ 0.31 and NH_4^+ = 0.15 $\pm$ 0.06). Values of nss $SO_4^=$ in the dust air mass (0.56 $\pm$ 0.06 μg m^{-3}) were similar to those measured in the SH marine tropics (0.52 $\pm$ 0.14 μg m^{-3}) and SH marine temperate regions (0.56 $\pm$ 0.12 μg m^{-3}). These are, in turn, within the range of values measured by *Andreae et al.* [1995] in a transect across the Atlantic along 19°S. The lowest mean concentration of nss $SO_4^=$ occurred in the NH marine air mass (0.15 $\pm$ 0.06 μg m^{-3}). Back trajectories for all of the marine air masses indicate that the sampled air had been over
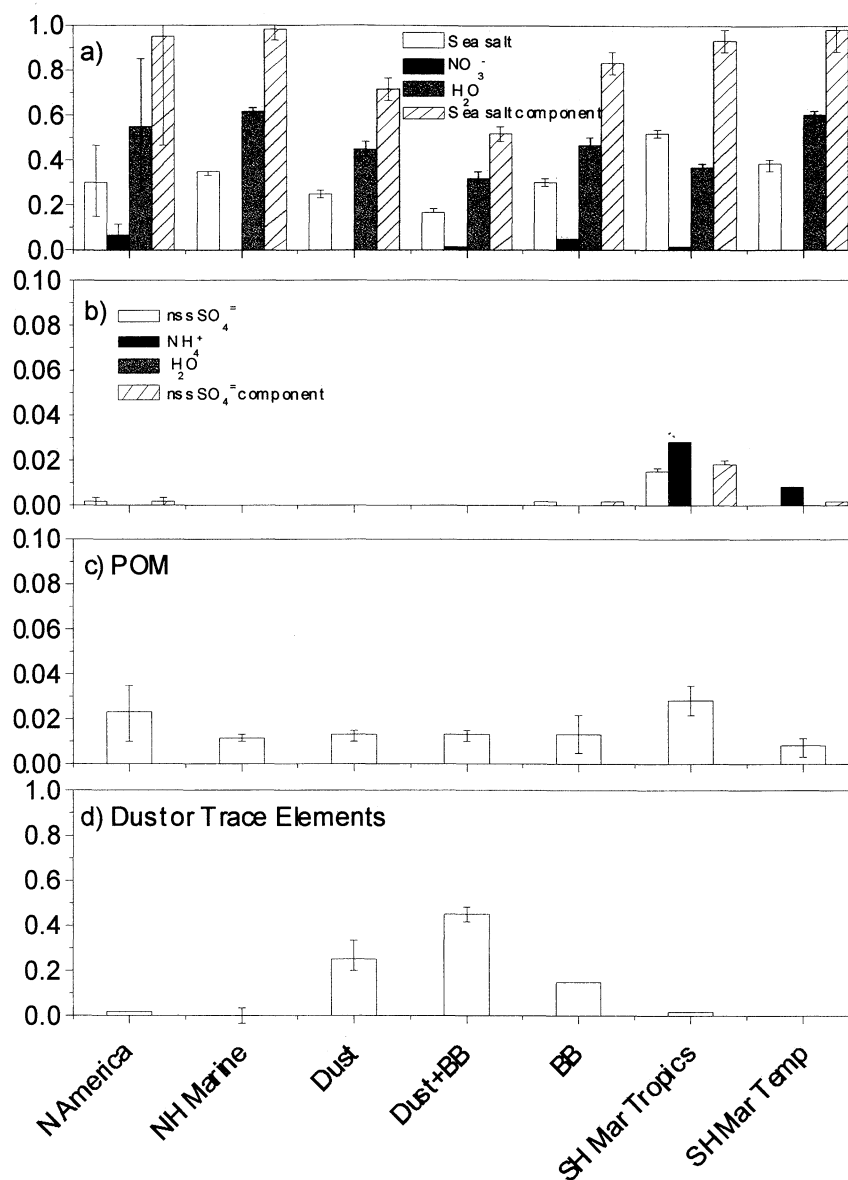
Figure 4. Mean supermicron ($1.1 < D_{50,aero} < 10 \ \mu m$ at 55% RH) mass fractions of the dominant chemical components for the seven air mass regions. Error bars indicate the uncertainty in the mean mass fraction for each region at the 95% confidence level. The number of samples available for the mass fraction calculation in each region is given in the Figure 3 caption.

the Atlantic for more than 6 days before reaching the ship. Seawater and atmospheric dimethylsulfide concentrations were, on average, 2 to 3 times higher in the SH than the NH marine air masses, however, indicating a stronger source of biogenic nss $SO_4^=$ in the Southern Hemisphere [*Bates et al.*, this issue].

Mass fractions and associated uncertainties at the 95% confidence level of the major submicron chemical species are shown in Figure 3. Mass fractions were calculated from the measured component mass concentration and the total aerosol mass concentration determined by gravimetric analysis. Three levels of sulfate aerosol contribution to the submicron mass are evident. Highest contributions were in the North America (67 ±

7.3%) and SH marine tropics (64 ± 1.9%) air mass regions. Contributions in the biomass burning and SH marine temperate air mass regions were lower (54 ± 12% and 44 ± 3.2%, respectively). Contributions in the NH marine (19 ± 9.9%), dust (24 ± 15%), and dust/biomass burning mixture (38 ± 15%) were lowest.

Supermicron nss $SO_4^=$ concentrations were low in all regions ($<0.09 \ \mu g \ m^{-3}$), while NH_4^+ concentrations were always below the detection limit of 0.001 $\mu g \ m^{-3}$. Supermicron mass fractions of nss $SO_4^=$ ranged from undetectable to 2% (Figure 4).

4.2.2. Sea salt and nitrate. Submicron sea-salt concentrations ranged between a mean of 0.08 and 0.22 $\mu g \ m^{-3}$ for all regions except for the dust air mass re-

gion where it averaged 0.39 ± 0.13 μg m^{-3}. The higher concentration was not due to an increase in wind speed but to a relatively low boundary layer height [*Bates et al.*, this issue]. These concentrations fall within the range of mean values measured for latitude bins of the Pacific spanning from 60°N to 70°S (0.11 to 0.58 μg m^{-3}) [*Quinn et al.*, 2000]. They are at the low end of the range reported for different air mass types in the northeast Atlantic during ACE 2 (0.34 to 0.88 μg m^{-3}) and considerably less than the mean value measured over the Southern Ocean during ACE 1 (1.0 ± 0.55 μg m^{-3}) [*Quinn et al.*, 2000, 1998].

Mass fractions of submicron sea salt were highest in the NH marine ($49 \pm 4.3\%$), dust ($49 \pm 6.4\%$), and SH marine temperate ($33 \pm 9.3\%$) air mass regions. The mean mass fraction was $21 \pm 7.3\%$ in the SH marine tropics region and less than 19% in the dust/biomass burning and the biomass burning air mass regions. Measured mean submicron sea-salt mass fractions for different latitude bands of the Pacific were similar, ranging from 7 to 27%. An exception to this was the 40° to 60°S region where the mean mass fraction was $53 \pm 3\%$ (mean and uncertainty at the 95% confidence level).

Supermicron mean sea-salt concentrations ranged between 4 and 10 μg m^{-3} for all air mass regions except that of dust where it was 19 ± 2.9 μg m^{-3}. Outside of the dust region these mean concentrations agree well with those measured for different air mass types during ACE 2 (4 to 10 μg m^{-3}) and with the mean ACE 1 supermicron concentration of 9.4 ± 5.5 μg m^{-3} [*Quinn et al.*, 2000, 1998].

Sea salt dominated the supermicron mass in all regions with mean mass fractions ranging from $52 \pm 3.6\%$ for the dust/biomass burning region to $98 \pm 5.2\%$ for the NH marine region. Lower values in the dust-containing regions are in contrast to the ACE 1 aerosol where, within the experimental uncertainty, supermicron sea salt made up 100% of the supermicron mass [*Quinn et al.*, 1998].

In regions where continental combustion emissions mix with sea salt, HNO$_3$ reacts with sea salt resulting in enhanced particulate NaNO$_3$ concentrations [*Roth and Okada*, 1998; *Gard et al.*, 1998]. Mean supermicron nitrate concentrations were highest in the North American air mass region (2.3 ± 1.6 μg m^{-3}) resulting in a mean mass fraction of $7.8 \pm 3.9\%$. The mean concentration in the biomass burning air mass region also was relatively high (0.94 ± 0.55 μg m^{-3}) with a mean mass fraction of $5.0 \pm 0.2\%$. In all other regions, the mean mass fraction was less than 3%.

4.2.3. Dust or trace elements. Dust concentrations are reported in the text as the mean and associated uncertainty at the 95% confidence level. For regions where more than two samples were collected, standard deviations (1σ) are given in Tables 1 and 2. Submicron dust concentrations averaged 0.73 ± 0.12 μg m^{-3} in the dust region and 0.68 ± 0.13 μg m^{-3} in the dust/biomass burning mixture. Mean submicron mass

fractions for the dust region and dust/biomass burning mixture were $22 \pm 3.3\%$ and $19 \pm 2.8\%$, respectively.

Outside of the dust regions, summed concentrations of the measured submicron trace elements averaged 0.02 μg m^{-3} in the North American, SH marine tropics, and SH marine temperate regions yielding mean mass fractions of 9% or less. Mean concentrations for the NH marine and biomass burning regions were near 0.1 μg m^{-3}, and the mean mass fractions were 8.9 ± 1.5 and $5.2 \pm 0.1\%$, respectively. The relatively large mass fraction for the NH marine air mass region was primarily due to Al, Si, and nonsoluble Mg.

Mean concentrations of supermicron dust in the dust and dust/biomass burning regions were 21 ± 3 and 24 ± 3.6 μg m^{-3}, respectively. These dust concentrations do not approach the values of up to several hundred micrograms per cubic meter reported for large-scale dust events across the Atlantic [e.g., *Li-Jones and Prospero*, 1998; *Chiapello et al.*, 1999]. The supermicron trace element mass in the biomass burning region also was assumed to be dust because of the similarity in the Al/Si and Fe/Si ratios for the dust, dust/biomass burning, and biomass burning regions (Table 2). The dust concentration in the biomass burning region was 1.9 ± 0.34 μg m^{-3}. Resulting mean mass fractions in the dust and dust/biomass mixture were 26 ± 3.9 and $45 \pm 6.7\%$, respectively. The mass fraction for the dust region is lower due to the high concentrations of sea salt. In the biomass burning region the mean mass fraction was $15 \pm 2.7\%$.

Supermicron mean values of trace elements ranged from 0.06 to 0.57 μg m^{-3} for the North American, NH marine, SH marine tropics, and SH marine temperate regions. Mean mass fractions for all of these regions were less than 2%.

4.2.4. POM. POM and BC concentrations are reported in the text as mean concentrations and associated uncertainties at the 95% confidence level. Mean submicron POM concentrations were highest in the North American (0.78 ± 0.17 μg m^{-3}) and biomass burning (0.48 ± 0.11 μg m^{-3}) air mass regions. Concentrations averaged about 0.2 μg m^{-3} in the NH marine, dust/biomass burning mixture, and SH marine temperate air masses. They were below the detection limit of 0.03 μg m^{-3} in the dust region and averaged 0.08 ± 0.04 μg m^{-3} in the SH marine tropics air mass region.

Mean submicron POM mass fractions were similar for the North America ($16 \pm 4\%$), biomass burning ($18 \pm 11\%$), and SH marine temperate ($12 \pm 6.4\%$) air mass regions. Mean mass fractions were about half of those for the NH marine ($8.7 \pm 1.8\%$), dust/biomass burning mixture ($6.6 \pm 2.2\%$), and the SH marine tropics ($5.7 \pm 2.2\%$). Mass fractions for the dust region were below detection limits.

For all air mass regions, supermicron mean POM concentrations were comparable to or higher than the submicron values. The size distribution of POM depends on the processes by which it is incorporated into

the aerosol particles. Its existence in the supermicron size range suggests that gas phase organics were adsorbed onto relatively large particles or it had a source in the ocean surface layer and was injected into the atmosphere in a manner similar to sea salt. Highest mean concentrations were measured in the North America (0.67 ± 0.16 μg m^{-3}), dust (1.0 ± 0.16 μg m^{-3}), and dust/biomass burning mixture (0.73 ± 0.14 μg m^{-3}) air mass regions. Mean concentrations ranged between 0.23 and 0.38 μg m^{-3} in the NH marine, biomass burning, SH marine tropics, and SH marine temperate regions. Though supermicron concentrations were higher than the corresponding submicron values, supermicron mass fractions were low for all regions ranging between 0.9 and 2.8%.

4.2.5. BC and nss K$^+$. Submicron mean concentrations of BC were significant only in the dust/biomass burning mixture and the biomass burning air mass regions (0.3 ± 0.02 and 0.35 ± 0.03 μg m^{-3}, respectively). In both of these regions, BC concentrations were higher than OC concentrations with OC/BC ratios of 0.33 (dust) and 0.71 (dust/biomass burning). Mean mass fractions in the dust/biomass burning and biomass burning air mass regions were $8.9 \pm 3.9\%$ and $6.7 \pm 1.3\%$, respectively. Mean mass fractions in all other regions were 2.1% or less.

BC concentrations were below detection limit (<0.01 μg m^{-3}) as were light absorption levels in the North America air mass region. These low levels of absorbing aerosol are in contrast to what was observed during the Tropospheric Aerosol Radiative Forcing Observational Experiment (TARFOX) conducted out of Wallops Island, Virginia, on the east coast of the United States. No direct measurement of BC concentration was made during TARFOX, but *Hegg et al.* [1997] report variable absorption coefficients (2.2 to 9.8 Mm^{-1}) and single scattering albedos (0.82 to 0.97) for altitudes less than 500 m. On the basis of back trajectories the North American air mass sampled during Aerosols99 had been over the western Atlantic for several days before being sampled on the ship [*Bates et al.*, this issue]. TARFOX focused on plumes of pollution haze freshly advected over the Atlantic Ocean [*Russell et al.*, 1999].

Aerosol nss soluble K$^+$ is a by-product of biomass burning and has been found to correlate well with BC concentrations [*Cachier et al.*, 1995]. As for black carbon, mean submicron nss K$^+$ concentrations were highest in the dust/biomass burning and biomass burning air mass regions (0.22 ± 0.08 and 0.24 ± 0.09 μg m^{-3}, respectively, mean and 1σ standard deviation). Mean mass fractions were $5.7 \pm 1.6\%$ (dust/biomass burning) and $5.5 \pm 1.0\%$ (biomass burning). In all other regions, mass fractions were 1.0% or less.

Mean concentrations of supermicron BC were above the detection limit for only the dust and dust/biomass burning air mass regions. Mean supermicron mass fractions for these regions were less than 0.1%. Similarly, mean mass fractions for supermicron nss K$^+$ were less than 0.1% for all regions.
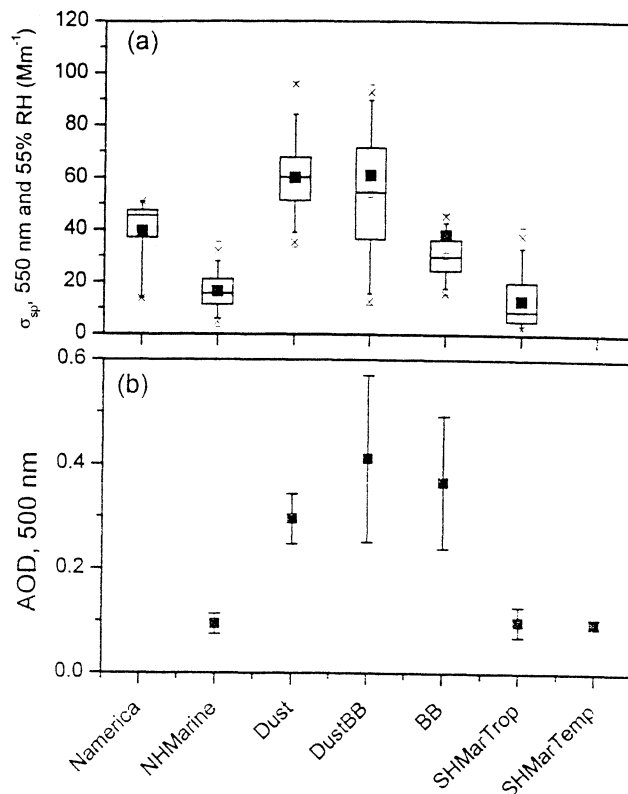

Figure 5. (a) Box plot of the aerosol scattering coefficient at 550 nm and 55% RH for the different air mass regions. Values are corrected for the angular response of the nephelometer and are reported at 0°C and 1013 mbar. The horizontal lines in the box denote the 25th, 50th, and 75th percentile values. The error bars denote the 5th and 95th percentile values. The two symbols above and below the ends of the error bars indicate the 0th and 1st and the 99th and 100th percentile values. The open square symbol in the box denotes the mean σ_{sp}. Solid boxes indicate the mean extinction ($\sigma_{sp} + \sigma_{ap}$). (b) Mean and standard deviation (1σ) of aerosol optical depth at 500 nm for the different air mass regions.

4.2.6. Other chemical components. Other chemical components that were detected but that contributed less than a few percent to the submicron mass were NO$_3^-$ (presumably associated with NH$_4^+$) and MSA$^-$. MSA$^-$ also was detected in the supermicron aerosol but made up less than 1% of the supermicron mass in all regions.

4.3. Regional Optical Properties

4.3.1. Aerosol scattering and backscattering coefficients. Mean values and percentile information for aerosol scattering coefficients at 550 nm and 55 $\pm$ 5% RH for the air mass regions are shown in Figure 5a. Because of instrument malfunction, measurements were not made in the SH marine temperate region.

Mean scattering coefficients at 550 nm were highest for the dust (60 $\pm$ 13 Mm^{-1}, mean and 1σ standard deviation) and dust/biomass burning air mass regions (54 $\pm$ 24 Mm^{-1}). Mean values were lower in the North
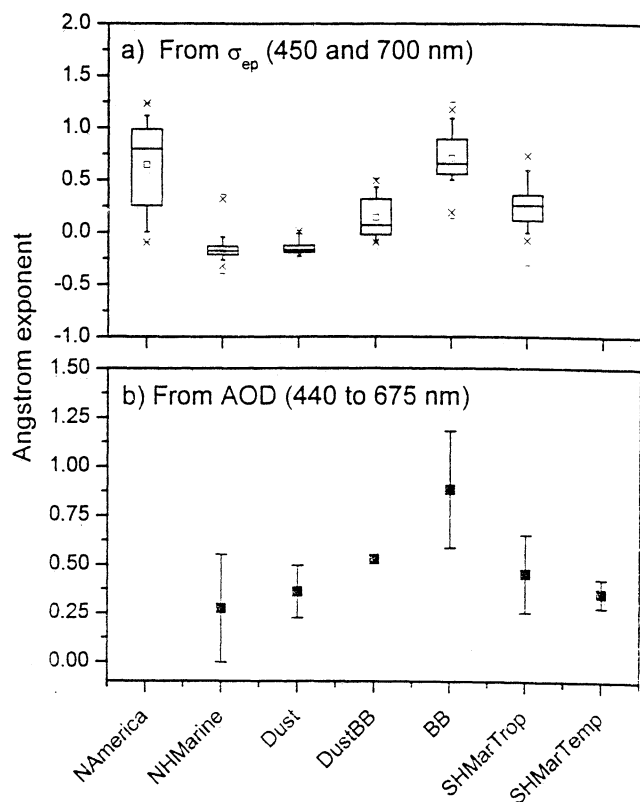
Figure 6. (a) Box plot of the Ångström exponent (450 and 700 nm wavelength pair) derived from the surface-measured scattering coefficient for $D_{aero} < 10$ μm at 55% RH. Percentile information is as described in the Figure 5 caption. (b) Mean and standard deviation (1σ) of the Ångström exponent (440 and 675 nm wavelength pair) derived from the measured column aerosol optical depth for the different air mass regions.

America (39 ± 13 Mm^{-1}) and biomass burning (30 ± 8.1 Mm^{-1}) regions. Lowest values were measured in the NH marine (16 ± 6.6 Mm^{-1}) and SH marine tropics (13 ± 9.9 Mm^{-1}) regions. For comparison, marine values measured during ACE 2 in the NE Atlantic and during ACE 1 in the Southern Ocean averaged 22 and 27 Mm^{-1}, respectively.

Mean backscatter coefficients show the same trend being highest for the dust (10 ± 2.2 Mm^{-1}) and dust/biomass burning air mass regions (8.9 ± 4.1 Mm^{-1}), about a factor of 2 lower for the North America (4.8 ± 2.7 Mm^{-1}) and biomass burning (4.6 ± 1.5 Mm^{-1}) regions, and lowest for the NH marine (2.9 ± 1.1 Mm^{-1}) and SH marine tropics (2.3 ± 1.4 Mm^{-1}) regions. The resulting backscattered fraction b ranged from a mean low of 0.10 ± 0.004 for the North America region to a mean high of 0.18 ± 0.10 for the NH marine region.

Mean Ångström exponents å for the 450 and 700 nm wavelength pair derived from

$$\text{å} = \frac{-\log\left(\frac{\sigma_{sp}(\lambda_1)}{\sigma_{sp}(\lambda_2)}\right)}{\log\left(\frac{\lambda_1}{\lambda_2}\right)} \quad (3)$$

are shown for the different air mass regions in Figure 6a. Since the nephelometer measurement included all particles with D_{aero} less than 10 μm, both the accumulation and coarse modes must be considered when interpreting values of å. The North America and biomass burning air mass regions had the highest mean values (0.64 ± 0.41 and 0.71 ± 0.21, respectively) indicating relatively more small diameter particles compared to the other regions. Surface area concentrations derived from the number size distribution (see Table 5) for the accumulation (S_{acc}) and coarse (S_{cs}) modes at 55% RH were 84 ± 23 and 87 ± 24 μm^2 cm^{-3}, respectively, for the North America region. For the biomass burning region, S_{acc} averaged 52 ± 13 μm^2 cm^{-3}, and S_{cs} averaged 17 ± 6.1 μm^2 cm^{-3}. In contrast, the dust/biomass burning region had a much lower mean å of 0.14 ± 0.19; the accumulation mode surface area concentration was considerably less than that of the coarse mode ($S_{acc} = 52 \pm 9.2$, and $S_{cs} = 78 \pm 17$ μm^2 cm^{-3}) . The dust region also had a low mean å (-0.15 ± 0.06) due to a large coarse mode ($S_{acc} = 11 \pm 2$, and $S_{cs} = 130 \pm 23$ μm^2 cm^{-3}). The mean value for the NH marine region was similar to the dust (-0.16 ± 0.1) due to a relatively small accumulation mode and persistent sea-salt coarse mode ($S_{acc} = 7.9 \pm 2.3$, and $S_{cs} = 75 \pm 21$ μm^2 cm^{-3}). The SH marine tropics region had a larger mean å of 0.26 ± 0.19 resulting from a relatively large accumulation mode ($S_{acc} = 19 \pm 5.6$, and $S_{cs} = 27 \pm 9.8$ μm^2 cm^{-3}). On the basis of the submicron mass fractions the accumulation mode in this region consisted primarily of nss SO$_4$ aerosol and a smaller POM and sea-salt component.

4.3.2. Aerosol absorption coefficient and single scattering albedo. Aerosol absorption coefficients were below the detection limit of 0.35 Mm^{-1} in all regions except the dust/biomass burning and biomass burning regions. These two regions also had the highest submicron BC concentrations. The range of absorption coefficients in the dust/biomass burning mixture was 2.1 to 11 Mm^{-1} with a mean and 1σ standard deviation of 7.1 ± 2.2 Mm^{-1}. For the biomass burning region the range was 0.68 to 13 Mm^{-1} with a mean and standard deviation of 7.5 ± 2.9 Mm^{-1}.

Single scattering albedo ω_o calculated as

$$\omega_o = \frac{\sigma_{sp}}{\sigma_{sp} + \sigma_{ap}} \quad (4)$$

is a measure of the relative magnitude of scattering and absorption by the aerosol. Here σ_{sp} is the nephelometer-measured scattering coefficient corrected for angular nonidealities as per equation (2), and σ_{ap} is the measured absorption coefficient corrected as per *Bond et al.* [1999]. Values of ω_o are reported at STP, 55% RH, and for particles with $D_{aero} < 10$ μm. For the dust/biomass burning region, ω_o ranged from 0.77 to 0.92 with a mean and 1σ standard deviation of 0.87 ± 0.05. For the biomass burning region, values ranged from 0.70 to 0.89 with a mean of 0.79 ± 0.04.
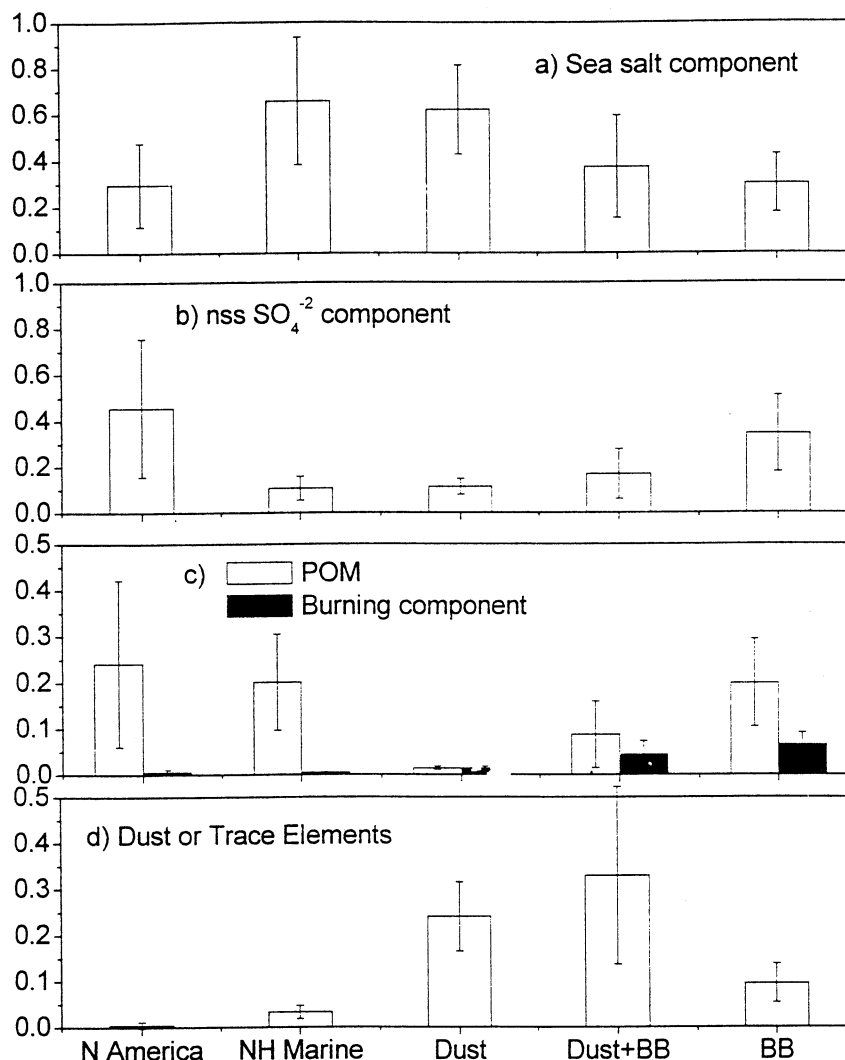
Figure 7. Mean fractional contribution of the submicron aerosol chemical components to extinction (scattering plus absorption) as a function of air mass region. Extinction fractions are reported at 55% RH. Error bars indicate the 1σ standard deviation of the mean.

4.3.3. Regional extinction due to individual aerosol chemical components. The fraction of the measured extinction (scattering plus absorption) due to the major aerosol chemical components was calculated at 55% RH using the method described in section 3.2. The major components considered are sea-salt aerosol which includes supermicron NO_3^- and water calculated to be associated with sea salt at 55% RH; sulfate aerosol which includes nss $SO_4^=$, NH_4^+, and water at 55% RH; a combustion component composed of BC, KNO_3, and K_2SO_4; POM; and dust (estimated from the measured Al concentration) or, outside of the African dust region, a sum of the measured trace elements. Results are shown for the submicron, supermicron, and sub-10 μm aerosol in Figures 7, 8, and 9. Extinction fractions are not shown for the SH marine tropics and SH marine temperate regions due to a lack of extinction closure and instrument malfunction, respectively. In general,

the trend in extinction fractions for each of the chemical components followed the trend in their mass fractions.

4.3.3.1. Sulfate aerosol: Submicron nss sulfate aerosol had the highest contribution to the submicron extinction in the North America air mass region (45 $\pm$ 30%, mean and 1σ standard deviation) This is also the region with the highest submicron mass fraction of sulfate aerosol resulting from emissions from the east coast of the United States. Extinction due to submicron sulfate aerosol was smaller in the biomass burning (34 $\pm$ 16%) region. It contributed to less than 17% of the submicron extinction in the NH marine, dust, and dust/biomass burning regions. The contribution of sulfate aerosol to supermicron extinction was minimal (<4%) in all regions. Mean nss sulfate aerosol contributions to extinction for sub-10 μm aerosol particles ranged from <2.2% (dust) to 20% (North America and biomass burning).
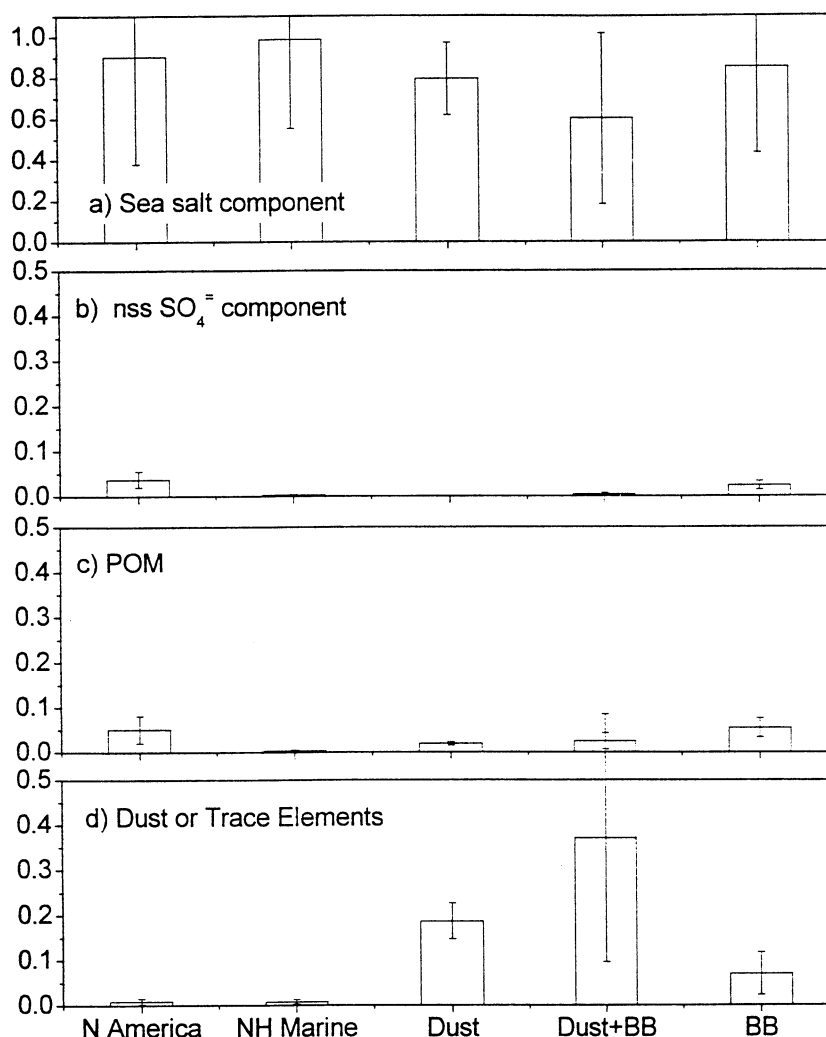
Figure 8. Mean fractional contribution of the supermicron aerosol chemical components to extinction (scattering plus absorption) as a function of the air mass region. Extinction fractions are reported at 55% RH. Error bars indicate the 1σ standard deviation of the mean.

4.3.3.2. Sea-salt aerosol: Sea-salt aerosol includes associated supermicron NO_3^- and water at 55% RH. Sea salt dominated the submicron extinction in the NH marine (66 ± 27%) and dust (62 ± 19%) regions. The dominance by sea salt is a result of relatively high concentrations, its propensity for water uptake with increasing RH, and its reluctance to release water with decreasing RH. As the relative humidity decreases from >70% to 55%, sea salt retains water to the extent that the wet particle mass is twice the dry mass [*Tang et al.*, 1997]. Sea salt contributed 37 ± 22% of the submicron extinction in the dust/biomass burning region. Contributions were lowest in the North America (29 ± 18%) and biomass burning (30 ± 13%) regions. These relatively large submicron sea-salt extinction fractions are consistent with what has been reported for the Pacific and Southern Oceans [*Quinn et al.*, 1996; *Quinn and Coffman*, 1999].

Sea salt dominated the supermicron extinction in all regions. Its contribution was lowest in the dust/biomass

burning mixture (60 ± 42%) due to relatively high dust concentrations. In all other regions the supermicron extinction fraction ranged from 79 to 98% with the largest contributions occurring in the NH marine region (98 ± 43%). Mean sea-salt aerosol contributions to extinction for sub-10 μm aerosol particles ranged from 52% (biomass burning) to 93% (NH marine).

4.3.3.3. Dust or trace elements: Dust contributed 24 ± 7.5% and 33 ± 9% to the submicron extinction in the dust and dust/biomass burning regions, respectively. In all other regions the submicron extinction due to a sum of the measured trace elements was less than 9% of the total.

Dust contributed 18 ± 3.9% and 37 ± 27% to the supermicron extinction in the dust and dust/biomass burning. Supermicron dust concentrations were similar in the two regions, but mean sea salt concentrations were a factor of 2.3 higher in the dust region. Hence the dust contribution to supermicron extinction was lower for the dust region. Dust in the biomass burning re-
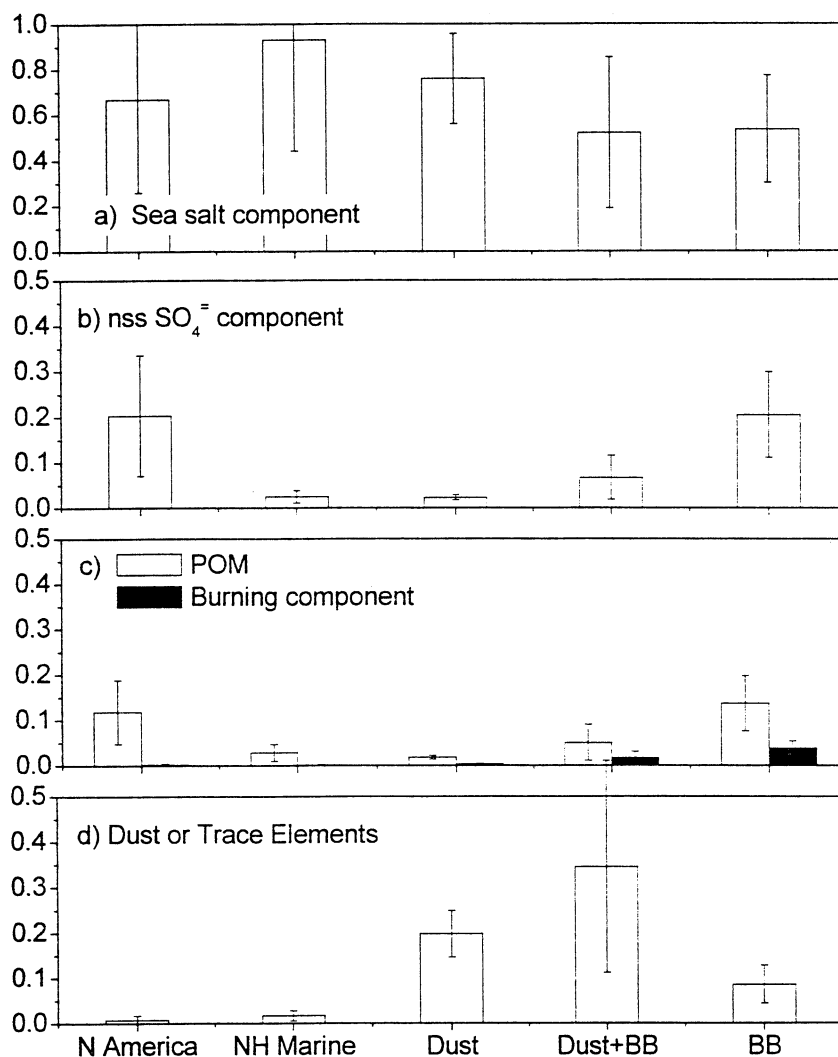
Figure 9. Mean fractional contribution of the total ($D_{\text{aero}} < 10 \ \mu$m) aerosol chemical components to extinction (scattering plus absorption) as a function of air mass region. Extinction fractions are reported at 55% RH. Error bars indicate the 1σ standard deviation of the mean.

gion contributed $6.9 \pm 4.7\%$ to the supermicron extinction. Mean dust contributions to extinction for sub-10 μm aerosol particles were 20, 34, and 8.5% for the dust, dust/biomass burning, and biomass burning regions, respectively.

These dust extinction fractions are similar to the monthly averaged dust scattering fractions reported for January (19%) and February (33%) 1994 at Barbados [*Li et al.*, 1996]. In contrast, *Li et al.* [1996] reported monthly averaged values of 50 to 70% for April and May, a time of year when outbreaks of African dust across the Atlantic are common.

4.3.3.4. POM: The POM submicron extinction fraction was $24 \pm 18\%$ for the North America region, $20 \pm 10\%$ for the NH marine region, and $20 \pm 9.5\%$ for the biomass burning region. Hence it appears to be a significant contributor to extinction in a wide range of air mass types. Its contribution was minimal ($<2\%$) in the dust region and 8.7% in the dust/biomass burning

region. POM contributed less than 5.5% to the supermicron extinction in all regions.

4.3.3.5. Black carbon and non-sea-salt potassium (burning component): Black carbon and nss K^+ associated with $SO_4^=$ and NO_3^- were grouped into a burning component. Extinction due to the entire component was then calculated. This component contributed $4.4 \pm 2.9\%$ to the submicron extinction in the dust/biomass burning region and $6.4 \pm 2.7\%$ in the biomass burning region. In all other regions, the contribution was less than 2%. The contribution to supermicron extinction was less than 1% in all regions.

4.3.4. Mass extinction efficiencies of the individual aerosol chemical components: Comparison of two methods. Mass extinction efficiencies, $\alpha_{ep,j}$, of individual aerosol chemical components are defined as

$$\alpha_{ep,j} = \frac{\sigma_{ep,j}}{m_j}, \tag{5}$$

QUINN ET AL.: DOMINANT AEROSOL CHEMICAL COMPONENTS

Table 6. Comparison of Mass Extinction Efficiencies Derived From Mie Calculations (Calculated) and From a Multiple Linear Regression (Empirical) at 550 nm[a]

Component	Empirical[b]		Calculated		Previously Reported Range
	Coefficient	Standard Error	Mean	Range	
Sea salt	2.2	0.3	1.6	1.1–2.4	0.61–2.1[c]
NSS $SO_4^=$ ion	5.7	2.1	4.0	3.1–5.2	4.2–7.5[c]
Dust or trace elements	0.9	0.1	1.1	0.7–1.8	1.07[d]
					0.73–0.79[e]
POM	2.7	4.2	3.3	1.3–5.4	2.6–3.6[f]
BC	3.6[g]	45	3.3	1.9–4.9	

[a]Values are for the size range $D_{aero} < 10$ μm (at 55% RH) and are means over the North America, NH marine, dust, dust/biomass burning, and biomass burning regions. Units are in m^2 g^{-1}.

[b]Based on equation (6), $r^2 = 0.95$, number of samples equal to 26.

[c]Pacific Ocean [*Quinn et al.*, 1996].

[d]Sal Island, 670 nm [*Chiapello et al.*, 1999].

[e]Barbados [*Li et al.*, 1996].

[f]Smoke particles in the smoldering phase [*Patterson and McMahon*, 1984; *Tangren*, 1982].

[g]From a regression that included only samples with measurable black carbon, $r^2 = 0.90$, number of samples equal to 9.

where $\sigma_{ep,j}$ is the extinction coefficient for component j and m_j is the mass of component j. An empirical and a calculational approach were used to calculate $\alpha_{ep,j}$ [*Charlson et al.*, 1999] for the size range $D_{aero} < 10$ μm (at 55% RH) to check for consistency between the methods. The empirical approach used a multiple linear regression of the mass concentration of the major chemical components against the extinction coefficient for the whole aerosol. The following equation was used to obtain weighted averages of the extinction efficiencies

$$\sigma_{ep} = \alpha_{ep,\text{sea salt}} m_{\text{sea salt}} + \alpha_{ep,\text{SO4,ion}} m_{\text{SO4,ion}}$$
$$+ \alpha_{ep,\text{dust}} m_{\text{dust}} + \alpha_{ep,\text{POM}} m_{\text{POM}} + \alpha_{ep,\text{BC}} m_{\text{BC}}, \quad (6)$$

where σ_{ep} is the sum of measured $\sigma_{sp} + \sigma_{ap}$ and the mass concentrations are a sum of the measured submicron and supermicron concentrations for each component. The "dust" component represents dust in the dust-containing regions and the sum of the trace elements in the other regions. The entire data set was used rather than deriving regional averages because of the small number of samples collected in some regions. The regression included both the submicron and supermicron size ranges as σ_{ep} was measured for $D_{aero} < 10$ μm. The calculational approach, based on the Mie calculation described in section 3.2, was used to calculate $\alpha_{ep,j}$ for the $D_{aero} < 10$ μm size range for comparison to the empirical approach.

Mean values from the two methods are compared in Table 6. For all components, $\alpha_{ep,j}$ calculated from the multiple linear regression falls within the range of values derived from the Mie calculation. The agreement between the two independent methods confirms the internal consistency in the data set and indicates that the derived parameters are accurate within experimental uncertainty.

4.3.5. Submicron and supermicron component mass extinction efficiencies. The calculational method also was used to calculate $\alpha_{ep,j}$ for the submicron and supermicron size ranges for the different air mass regions. In these calculations, sea salt and NO_3^- in the supermicron size range were combined to form the sea-salt component, and nss $SO_4^=$ was combined with NH_4^+ to form the sulfate aerosol component. Both of these components also included the mass of water calculated to be associated with them at 55% RH. The value of $\alpha_{ep,j}$ also was calculated for the nss sulfate ion such that $\sigma_{ep,j}$ is the scattering due to sulfate aerosol (nss $SO_4^=$, NH_4^+, and water at 55% RH) and m_j is the mass of the nss $SO_4^=$ ion. The value of $\alpha_{ep,j}$ for the nss $SO_4^=$ ion is a useful quantity as chemical transport models predict the ion concentration or column burden of sulfate rather than the sulfate aerosol concentration [e.g., *Langner and Rodhe*, 1991]. Mean values are reported in Table 7 for the different air mass regions.

Mean mass extinction efficiencies of submicron sea salt ranged from 5.2 to 6.6 m^2 g^{-1} and of supermicron sea salt ranged from 0.9 to 1.4 m^2 g^{-1}. These compare well with values estimated for latitude bands of the central Pacific. For the Pacific, mean submicron values ranged from 3.5 to 7.7 m^2 g^{-1}, and supermicron values ranged from 0.39 to 1.1 m^2 g^{-1} for the aerosol at 30% RH [*Quinn et al.*, 1996].

Mean $\alpha_{ep,j}$ for submicron nss $SO_4^=$ aerosol ranged from 2.6 to 4.3 m^2 g^{-1} and for submicron nss $SO_4^=$ ion ranged from 3.3 to 5.8 m^2 g^{-1}. These values also are comparable to those reported for latitude bands of the central Pacific (4.2 to 7.5 m^2 g^{-1}). In addition, they fall within the theoretical range of low-RH sulfate scattering efficiencies predicted by *Charlson et al.* [1999].

Mass extinction efficiencies for submicron dust in the

Table 7. Mean and Standard Deviation (1σ) of the Mass Extinction Efficiencies of the Major Chemical Components in Each Air Mass Region[a]

Region	Sea Salt[b]		NSS Sulfate Ion[c]		NSS Sulfate Aerosol[d]		Dust or Trace Elements		POM		BC and nss K[+e]		Total Aerosol	
	mean	s.d.	mean	s.d.	mean	s.d.	mean	s.d.	mean	s.d.	mean	s.d.	mean	s.d.
Submicron, $m^2\ g^{-1}$														
North America	5.2	3.5	4.1	2.1	3.4	2.1	2.8	1.7	5.0	3.1	2.7	1.7	4.1	2.7
NH marine	5.4	0.9	4.6	0.6	3.9	0.6	2.9	0.4	5.5	0.56	3.1	0.1	5.0	0.8
African dust	5.9	1.0	3.3	0.4	2.6	0.5	3.5	0.6	7.1	1.0	3.2	0.5	4.6	0.7
African dust/BB	6.9	1.4	4.2	0.7	3.1	0.7	4.3	0.9	7.5	1.4	5.5	1.2	5.0	1.0
Biomass burning	6.6	1.5	5.8	0.9	4.3	0.9	4.5	0.9	6.9	1.4	5.7	1.1	5.4	1.1
Supermicron, $m^2\ g^{-1}$														
North America	0.9	0.4					0.6	0.2	1.6	0.4			1.0	0.4
NH marine	1.0	0.3					0.7	0.2	1.9	0.2			1.0	0.3
African dust	1.2	0.2					0.5	0.1	1.1	0.1			1.0	0.1
African dust/BB	1.3	0.4					0.6	0.2	1.8	0.5			1.0	0.3
Biomass burning	1.2	0.4					0.6	0.2	2.1	0.5			1.1	0.3

[a]Integral values are reported at 55% RH for the submicron ($D_{aero} < 1.1\ \mu m$) and supermicron ($1.1 < D_{aero} < 10\ \mu m$) size ranges. Values are based on a Mie calculation; s.d., standard deviation.
[b]Includes NO_3^- and water at 55% RH.
[c]Includes scattering due to nss $SO_4^=$, NH_4^+, and water at 55% and mass due to nss $SO_4^=$ ion.
[d]Includes scattering due to nss $SO_4^=$, NH_4^+, and water at 55% and mass due to nss $SO_4^=$, NH_4^+, and water at 55% RH.
[e]Here nss K^+ with associated $SO_4^=$ and NO_3^-.

dust region averaged 3.5 ± 0.6 $m^2\ g^{-1}$ and in the dust/biomass burning region averaged 4.3 ± 0.9 $m^2\ g^{-1}$. Supermicron values averaged 0.5 ± 0.1 and 0.6 ± 0.2 $m^2\ g^{-1}$ for the dust and dust/biomass burning regions, respectively.

Mean submicron POM mass extinction efficiencies ranged from 5.0 to 7.5 $m^2\ g^{-1}$ over all regions. Supermicron values ranged from 1.1 to 2.1 $m^2\ g^{-1}$. Because of a lack of information of the hygroscopicity of the sampled organic matter, no water was associated with the POM. By assuming that the water uptake by POM is similar to that of sulfate aerosol, *Liousse et al.* [1996] calculated an increase in $\alpha_{ep,j}$ from 4 for a dry aerosol to 6.8 $m^2\ g^{-1}$ for an aerosol at 80% RH due to an increase in particle size. The competing effect of lowering the refractive index must also be considered, however. Mean submicron mass extinction efficiencies for the burning component (BC plus submicron KNO_3 and K_2SO_4) ranged from 2.7 to 5.7 $m^2\ g^{-1}$.

4.3.6. Aerosol optical depth: Regional values of τ_a. Mean aerosol optical depths (500 nm) τ_a are compared to surface scattering and extinction coefficients (550 nm) in Figure 5. Measurements of τ_a were not made at the beginning of the cruise for the North America air mass region due to extensive cloud cover. Relatively low values were measured in the NH marine (0.09 ± 0.02, mean and 1σ standard deviation), SH marine tropics (0.1 ± 0.03), and SH marine temperate (0.1 ± 0.01) regions. These values are on the

low end of the range reported for the Atlantic Ocean [*Smirnov et al.*, 1995]. Highest mean τ_a were measured in the dust/biomass burning (0.41 ± 0.16) and biomass burning (0.36 ± 0.13) regions with the mean τ_a in the dust region being lower (0.29 ± 0.05).

To compare values of surface extinction and τ_a, a linear regression of τ_a against surface extinction was performed on a regional basis. All regions display a linear relationship, but the slope varies (Figure 10a). The variation in slope appears to be a function of the vertical distribution of the aerosol. The NH marine region and second half of the SH marine tropics region were periods along the cruise track where, based on trajectories and profiles of 180° backscatter from a micropulse lidar, the aerosol was confined primarily to the marine boundary layer (MBL). Here the slope of the regression line is the lowest (0.002). The coefficient of determination of the regression, r^2, for these regions is 0.53. In the dust region, trajectories arriving at 500 and 2500 m indicate that dust was transported out of Africa to the mid Atlantic primarily in the MBL. Lidar profiles show an aerosol layer above the MBL but that the bulk of the aerosol backscattering was within the MBL [*Voss et al.*, this issue (b)]. Here the slope of the regression line is at an intermediate value (0.003), and r^2 equals 0.55. There were not enough observations of τ_a in the dust/biomass burning region to define a relationship between τ_a and surface extinction. In the biomass burning region, transport out of Africa occurred primarily above
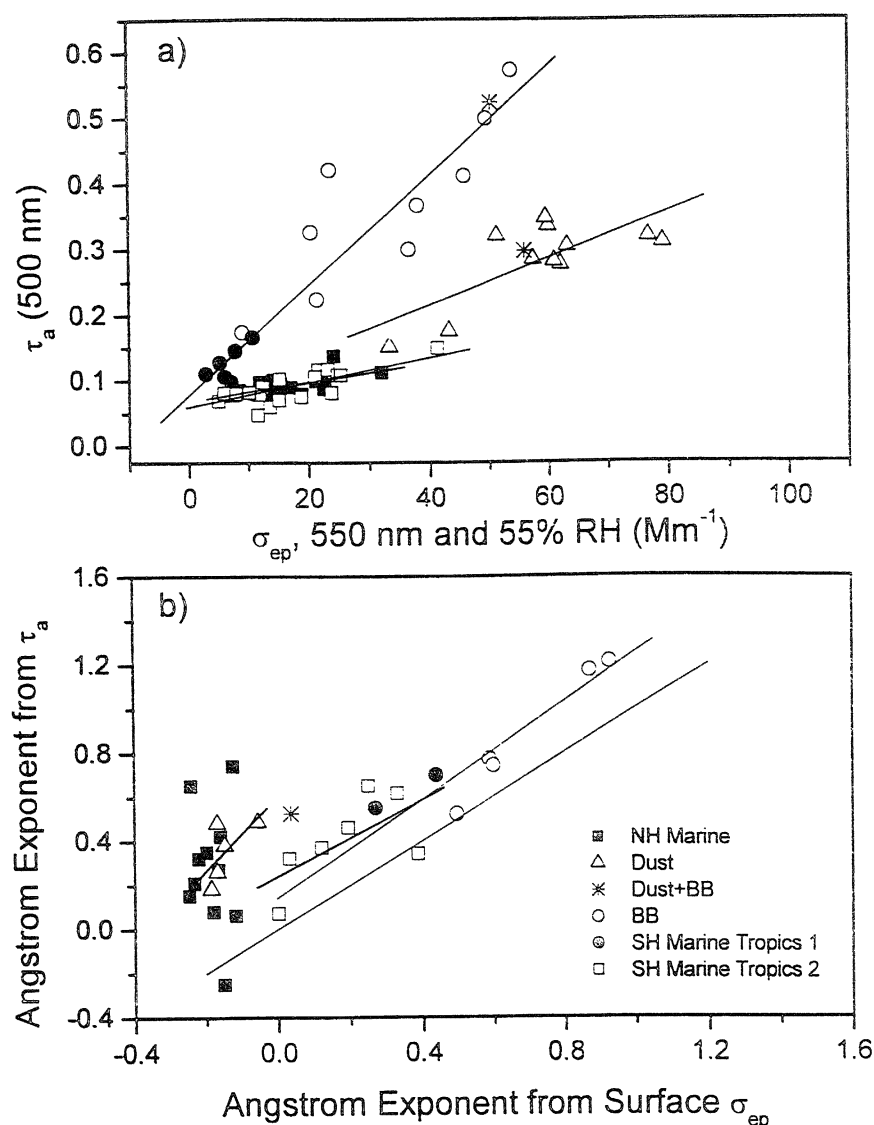
Figure 10. (a) Linear regression of measured τ_a (500 nm) against measured surface extinction ($\sigma_{sp} + \sigma_{ap}$ at 550 nm and 55% RH). Lines represent the linear fit line for all data within the indicated regions. (b) Linear regression of the Ångström exponent derived from τ_a (440 and 675 nm) against the Ångström exponent derived from surface-measured σ_{sp} (450, 700 nm). The dashed line is the one-to-one line.

500 m. The 2500 m arrival height trajectories indicate flow from southwestern North Africa. On the basis of lidar profiles, aerosol was mixed up to at least 4 km with multiple layers throughout. In the first portion of the SH marine tropics region, trajectories arriving at 500 m had been over the ocean for up to 6 days prior to reaching the ship. Upper level flow, however, continued to be from over Africa contributing to an aerosol layer above the MBL reaching up to 4 km. Combining the biomass burning and first portion of the SH marine tropics regions results in the largest slope value (0.008) and the largest r^2 (0.88).

Differences in the surface and column-integrated aerosol size distributions can be inferred from Ångström exponents derived from surface scattering coefficients ver-

sus those derived from τ_a. Values of å derived from τ_a over a wavelength range of 440 to 700 nm were higher than those based on surface scattering coefficients (450 and 700 nm) for all air mass regions (Figure 6). This difference is most likely due to a smaller fraction of coarse mode particles in the atmospheric column relative to the coarse sea-salt fraction that persists in the boundary layer. A linear regression of mean Ångström exponents derived from τ_a against those derived from surface σ_{ep} is shown in Figure 10b. Two regions with large coarse mode surface area concentrations (dust and NH marine, see Table 5) show a narrow range of å values derived from surface σ_{sp} with a broader range derived from τ_a. This difference results in a greater departure from the one-to-one line than is found in the other re-

gions. The correlation for the second portion of the SH marine tropics, where the aerosol was confined to the MBL and there was a relatively large accumulation mode, results in a slope similar to the one-to-one line with an r^2 value of 0.41. Regions with the largest å (biomass burning and the first portion of the SH marine tropics) show the best correlation ($r^2 = 0.88$). For at least the biomass burning region it may be that the aerosol from the upper troposphere maintained its size distribution as it was mixed into the MBL.

4.3.7. Fraction of τ_a due to aerosol extinction in the MBL.

To estimate the fraction of the measured τ_a due to aerosol extinction in the MBL, the aerosol optical depth of the MBL, $\tau_{a,\mathrm{MBL}}$, was calculated using three approaches. Because of the methodology involved, all three methods were restricted to times when surface extinction, RH profiles, and aerosol optical depth were measured simultaneously. In the first method (Integrated Surface Extinction), in situ scattering and absorption coefficients measured at the surface were extrapolated through the MBL using the following equation:

$$\tau_{\mathrm{mbl}} = \int_0^z (\sigma_{sp} \times f(\mathrm{RH}) + \sigma_{ap})dz, \qquad (7)$$

where z is the top of the MBL defined by the beginning of a strong negative gradient in RH and/or the temperature inversion. In cases where there was no well-defined MBL, micropulse lidar (MPL) profiles of 180° backscatter were used to determine the height of the lowest aerosol layer (see *Voss et al.* [this issue (b)] for more details of the MPL measurements). This method assumes that the aerosol measured at the surface is uniformly mixed through the MBL and that there are no gradients in aerosol chemical composition or size distribution. The extinction measured at 55% RH was adjusted to ambient RH using vertical soundings of RH and previously measured $f(\mathrm{RH})$ relationships. For the marine air mass regions, $f(\mathrm{RH})$ measured during onshore flow at Cape Grim, Tasmania, was used [*Carrico et al.*, 1998]. For the continentally influenced air mass regions, two $f(\mathrm{RH})$ relationships were used for comparison. These were measured during continental flow at Sable Island, Nova Scotia (Integrated Surface Extinction 1) [*McInnes et al.*, 1998] and at the Kaashidhoo Climate Observatory in the Indian Ocean (Integrated Surface Extinction 2) (J. Ogren, personal communication, 1999). The two $f(\mathrm{RH})$ relationships for continentally influenced aerosol resulted in comparable values of $\tau_{a,\mathrm{MBl}}$ (see Figure 11). For σ_{ap}, $f(\mathrm{RH})$ was assumed to be one.

The second method (Integrated Lidar Extinction) was independent from the first and involved integrating the lidar extinction from 75 m to the top of the lowest aerosol layer defined by a sharp decrease in extinction. Under conditions of a well-defined MBL, the top of the lowest aerosol layer corresponded in most cases to the
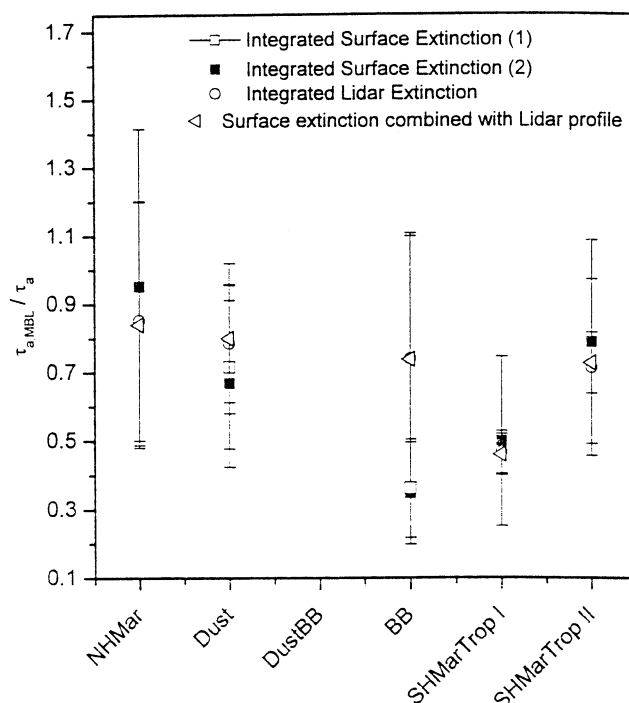

Figure 11. Fraction of column-measured aerosol optical depth due to aerosol in the MBL (mean and 1σ standard deviation) calculated with three different methods: Integrated Surface Extinction (1 and 2 indicate use of the previously measured Sable Island and Kaashidhoo $f(\mathrm{RH})$ relationships, respectively; Integrated Lidar Extinction; and Surface Extinction combined with the Lidar profile.

top of the MBL. This method assumes that the lidar extinction to backscatter ratio, S_a, is constant.

The third method used information from the surface extinction and lidar measurements. In this method (Surface Extinction Combined With Lidar Profile) the vertical profile of aerosol extinction within the MBL was estimated from the lidar-derived extinction profile as follows. The lidar-derived extinction $\sigma_{ep,\mathrm{MPL}}$ at height z within the MBL was normalized by $\sigma_{ep,\mathrm{MPL}}$ at 75 m, the lowest height of the lidar retrieval. This ratio was then scaled by the surface extinction coefficient determined from measured scattering and absorption coefficients to calculate τ_a [*Bergin et al.*, 2000]

$$\tau_{a,\mathrm{MBL}} = (\sigma_{sp} \times f(\mathrm{RH}) + \sigma_{ap}) \int_0^z \frac{\sigma_{ep,\mathrm{MPL}}(z)}{\sigma_{ep,\mathrm{MPL}}(75)} dz. \quad (8)$$

The $f(\mathrm{RH})$ relationships discussed above (Cape Grim for marine regions and Kaashidoo for continentally influenced regions) were applied. This method also assumes that the lidar extinction to backscatter ratio, S_a, is constant. It agreed well with the Integrated Lidar Extinction method in all regions.

Figure 11 shows the fraction of τ_a due to $\tau_{a,\mathrm{MBL}}$ estimated by the three methods. For the NH marine region the two independent methods agreed within 10%. On

the basis of the Integrated Surface Extinction method, $95 \pm 46\%$ (mean and 1σ standard deviation) of τ_a was due to aerosol in the MBL. Lower values are due to the occurrence of an aerosol layer above the MBL as observed by the MPL at $23.61°N, 54.96°W$. In the dust region the two independent methods agreed within 18%. On the basis of the Integrated Surface Extinction, $67 \pm 24\%$ of τ_a was due to aerosol in the MBL. No sunphotometer aerosol optical depth measurements were made at the same time as radiosonde launches during the dust/biomass burning region, so no attempt was made to calculate the fraction of τ_a due to aerosol in the MBL.

The SH marine tropics region was split into two periods for this analysis. For both periods the agreement between the two independent methods was within 10%. During the first portion of the period, the MBL extended to 1.5 km, while the MPL extinction profiles showed an upper aerosol layer extending to near 4.0 km. Upper layer 6-day back trajectories showed transport from Africa to the region. The estimated fraction of τ_a due to MBL aerosol was $50 \pm 25\%$. During the second portion of the period, no upper aerosol layer was detected, and the MBL aerosol was estimated to make up $80 \pm 30\%$ of τ_a.

In the biomass burning region, $\tau_{a,MBL}$ estimated from the Integrated Lidar Extinction Method ($74 \pm 37\%$) was a factor of 2 higher than that estimated from Integrated Surface Extinction ($35 \pm 15\%$). The aerosol in this region, which reached up to 4 km, consisted of multiple layers. The assumption required by the Integrated Surface Extinction method that the aerosol was well-mixed throughout most likely was not appropriate. Layers of higher aerosol burdens and therefore τ_a may have been present aloft. It is interesting that this is the same region that showed the best agreement between measured surface and column Ångström exponents indicating a similarity in surface and column aerosol properties.

Nephelometer measurements were not made during the SH marine temperate region. However, the MPL extinction profiles coupled with the soundings indicate that all detectable aerosol was contained with the MBL.

5. Conclusions

The Aerosols99 cruise across the Atlantic from Norfolk, Virginia to Cape Town, South Africa, in January and February of 1999 provided the opportunity to characterize the properties of relatively pristine marine aerosol, aerosol impacted by anthropogenic emissions from North America, and dust and biomass burning emissions from Africa. In all, seven "air mass" regions were encountered: North America, NH marine, dust, a mixture of dust and biomass burning, biomass burning, SH marine tropics, and SH marine temperate. In situ measurements were made of aerosol chemical composition (inorganic ions, organic carbon, black carbon, and trace elements), number size distribution, and scattering, backscattering, and absorption coefficients.

In addition, to provide information about the aerosol through the atmospheric column, measurements were made of aerosol optical depth and vertical profiles of aerosol backscatter. From these data, submicron and supermicron mass fractions of the major chemical components, the extinction due to those components, mass extinction efficiencies of the components, and the fraction of the measured column aerosol optical depth due to aerosol in the boundary layer were estimated.

Submicron nss $SO_4^=$ aerosol made up a significant portion of the submicron aerosol mass in all air mass regions with mass fractions ranging from 20 to 67% (at 55% RH). Largest mass fractions were in the North America and SH marine tropics regions due to anthropogenic and biogenic emissions, respectively. Contribution of nss $SO_4^=$ to submicron extinction ranged from 10% to 45% (at 55% RH) with the highest value in the North America region. For aerosol with D_{aero} less than 10 μm, nss $SO_4^=$ aerosol made up 2.2 to 20% of the sub-10 μm extinction. Estimated mean mass extinction efficiencies for submicron nss $SO_4^=$ aerosol ranged from 2.6 to 4.3 m^2 g^{-1} (at 55% RH).

Sea-salt mean submicron mass fractions ranged from 9 to 49% for the different air mass regions. Mean contributions to submicron extinction ranged from 29 to 66%. Mean supermicron mass fractions ranged from 52 to 98% with the smallest values in the air mass regions containing dust and the largest values in more pristine marine regions. Contributions to supermicron extinction ranged from 60 to 98%. Sea salt made up 52 to 93% of the sub-10 μm extinction thereby dominating the sub-10 μm extinction in all regions including those influenced by continental sources. The dominance of extinction by sea salt results from its propensity to take up water with increasing RH and its reluctance to release water with decreasing RH. Mean submicron sea-salt mass extinction efficiencies ranged from 5.2 to 6.9 m^2 g^{-1}, and supermicron values ranged from 0.9 to 1.3 m^2 g^{-1}.

Mean submicron mass fractions of dust in the dust and dust/biomass burning regions were $22 \pm 3.3\%$ (mean and uncertainty at the 95% confidence level) and $19 \pm 2.8\%$, respectively. Mean supermicron mass fractions were $26 \pm 3.9\%$ and $45 \pm 6.7\%$, respectively. The lower mass fraction in the dust region is due to relatively high sea-salt concentrations. Mean contributions of dust to submicron extinction were $24 \pm 7.5\%$ and $33 \pm 20\%$ in the dust and dust/biomass burning regions, respectively. In the supermicron size range, dust contributed $18 \pm 3.9\%$ and $37 \pm 27\%$ to extinction in the dust and dust/biomass burning regions, respectively. Dust made up 20 to 34% of the sub-10 μm extinction in the dust-containing regions. Submicron mass extinction efficiencies for dust averaged 3.6 m^2 g^{-1}, and supermicron values averaged 0.6 m^2 g^{-1}.

Submicron mass fractions of POM ranged from below detection limit in the dust region to $18 \pm 5.7\%$ in the biomass burning region. Its contribution to submicron extinction ranged from below detection limits to

24%. Supermicron mass fractions were less than 2.3% for all regions. Submicron mass extinction efficiencies for POM ranged from 5.0 to 7.5 m^2 g^{-1}. In the biomass burning region the black carbon mean submicron mass fraction was 6.7 $\pm$ 2.1% with a contribution of 6.4 $\pm$ 2.7% to the submicron extinction.

Mean aerosol optical depths at 500 nm for the different air mass regions ranged from a low of 0.09 in the marine regions to 0.41 in the dust/biomass burning region. The portion of the measured column aerosol optical depth due to aerosol in the MBL was estimated with two independent methods. In regions with a well defined MBL and no aerosol layer aloft (NH marine and SH marine tropics), the measured τ_a was accounted for by aerosol extinction in the MBL. In all other regions there was an aerosol layer above the MBL, and contributions of MBL aerosol to column τ_a ranged from regional means of 35 to 67%.

The Aerosols99 data set provides evidence for large regional variations in the concentrations, mass fractions, and extinction fractions of the dominant aerosol chemical components. This variability in chemical components translates into large regional variations in aerosol extinction coefficients measured at the surface, aerosol optical depth, and single scattering albedo. The variability presented here is representative of the Atlantic Ocean during January and February (a time of year when biomass burning emissions are at a maximum in northern Africa and dust emissions are at a minimum) and should therefore serve to improve climatologies of aerosols for this season. The observed variability also indicates the need for a focus on regional aerosol properties and the limitations of a focus on globally and annually averaged aerosol properties in estimates of aerosol radiative forcing.

Although the measurements made on the cruise were relatively thorough, it was necessary to assume the size distribution of dust and OC and a factor to convert OC into POM. In addition, no information was available on the hygroscopicity of the sampled POM. Ideally, future experiments will include the measurement of the size distribution of all major aerosol chemical components. In addition, speciation of the aerosol organic matter would help in determining its hygroscopicity, OC to POM conversion factors, and the processes that result in its incorporation into submicron and supermicron aerosol.

References

Anderson, T. L., and J. A. Ogren, Determining aerosol radiative properties using the TSI 3563 integrating nephelometer, *Aerosol Sci. Technol., 29,* 57–69, 1998.

Anderson, T. L., D. S. Covert, J. D. Wheeler, J. M. Harris, K. D. Perry, B. E. Trost, D. J. Jaffe, and J. A. Ogren, Aerosol backscatter fraction and single scattering albedo: Measured values and uncertainties at a coastal station in the Pacific Northwest, *J. Geophys. Res., 104,* 26,793–26,807, 1999.

Andreae, M. O., W. Elbert, and S. J. de Mora, Biogenic sulfur emissions and aerosols over the tropical South Atlantic, 3, Atmospheric dimethylsulfide, aerosols, and cloud condensation nuclei, *J. Geophys. Res., 100,* 11,335–11,356, 1995.

Ayers, G. P., M. D. Keywood, and J. L. Gras, TEOM vs. manual gravimetric methods for determination of PM2.5 aerosol mass concentrations, *Atmos. Environ., 33,* 3717–3721, 1999.

Bates, T. S., P. K. Quinn, D. J. Coffman, J. E. Johnson, T. L. Miller, D. S. Covert, A. Wiedensohler, S. Leinert, A. Nowak, and C. Neusüss, Regional physical and chemical properties of the marine boundary layer aerosol across the Atlantic during Aerosols99: An overview, *J. Geophys. Res.,* this issue.

Bergin, M. H., S. E. Schwartz, R. N. Halthore, J. A. Ogren, and D. L. Hlavka, Comparison of aerosol optical depth inferred from surface measurements with that determined by Sun photometry for cloud-free conditions at a continental U.S. site, *J. Geophys. Res., 105,* 6807–6816, 2000.

Berner, A., C. Lurzer, F. Pohl, O. Preining, and P. Wagner, The size distribution of the urban aerosol in Vienna, *Sci. Total Environ., 13,* 245–261, 1979.

Bond, T. C., T. L. Anderson, and D. Campbell, Calibration and intercomparison of filter-based measurements of visible light absorption by aerosols, *Aerosol Sci. Technol., 30,* 582–600, 1999.

Bray, W. H., Water vapor pressure control with aqueous solutions of sulfuric acid, *J. Mater., 5,* 233–248, 1970.

Bromley, L. A., Thermodynamic properties of strong electrolytes in aqueous solutions, *AIChE J., 19,* 313–320, 1973.

Cachier, H., C. Liousse, P. Buat-Menard, and A. Gaudichet, Particulate content of savanna fire emissions, *J. Atmos. Chem., 22,* 123–148, 1995.

Carrico, C. M, M. J. Rood, and J. A. Ogren, Aerosol light scattering properties at Cape Grim, Tasmania, during the First Aerosol Characterization Experiment (ACE 1), *J. Geophys. Res., 103,* 16,565–16,574, 1998.

Charlson, R. J., T. L. Anderson, and H. Rodhe, Direct climate forcing by anthropogenic aerosols: Quantifying the link between atmospheric sulfate and radiation, *Contrib. Atmos. Phys., 72*(1), 79–94, 1999.

Chiapello, I., G. Bergametti, B. Chatenet, F. Dulac, I. Jankowiak, C. Liousse, and E. S. Soares, Contribution of the different aerosol species to the aerosol mass load and optical depth over the northeastern tropical Atlantic, *J. Geophys. Res., 104,* 4025–4035, 1999.

Clegg, S. L., and P. Brimblecombe, Potential degassing of hydrogen chloride from acidified sodium chloride droplets, *Atmos. Environ., 19,* 465–470, 1985.

Cohen, M. D., R. C. Flagan, and J. H. Seinfeld, Studies of concentrated electrolyte solutions using the electrodynamic balance, 1, Water activities for single-electrolyte solutions, *J. Phys. Chem., 91,* 4563–4574, 1987.

Covert, D. S., A. Wiedensohler, and L. M. Russell, Particle charging and transmission efficiencies of aerosol charge neutralizers. *Aerosol Sci. Technol., 27,* 208–214, 1997.

Draxler, R. R., Hybrid Single-Particle Lagrangian Integrated Trajectories (HY-SPLIT): Version 3.0 user's guide and model description, *Tech. Rep. ERL ARL-195,* Natl. Oceanic and Atmos. Admin., Silver Spring, Md., 1992.

Feely, R. A., G. J. Massoth, and G. T. Lebon, Sampling of marine particulate matter and analysis by X-ray fluo-

rescence spectrometry, in *Marine Particles: Analysis and Characterization, Geophys. Monogr. Ser.*, vol. 63, edited by D. C. Hurd and D. W. Spencer, pp. 251–257, AGU, Washington, D.C., 1991.

Feely, R. A., E. T. Baker, G. T. Lebon, J. F. Gendron, G. J. Massoth, and C. W. Mordy, Chemical variations of hydrothermal particles in the 1996 Gorda Ridge Event and chronic plumes, *Deep Sea Res., 45*, 2637–2664, 1998.

Gard, E., et al., Direct observation of heterogeneous chemistry in the atmosphere, *Science, 279*, 1184–1187, 1998.

Hegg, D. A., J. Livingston, P. V. Hobbs, T. Novakov, and P. Russell, Chemical apportionment of aerosol column optical depth off the mid-Atlantic coast of the United States, *J. Geophys. Res., 102*, 25,293–25,303, 1997.

Holland, H. D., *The Chemistry of the Atmosphere and Oceans*, p. 154, John Wiley, New York, 1978.

Intergovernmental Panel on Climate Change (IPCC), *Climate Change 1995*, edited by J. T. Houghton et al., Cambridge Univ. Press, New York, 1996.

Langner, J., and H. Rodhe, A global three-dimensional model of the tropospheric sulfur cycle, *J. Atmos. Chem., 13*, 225–263, 1991.

Li, X., D. Savoie, K. Voss, and J. M. Prospero, Dominance of mineral dust in aerosol light-scattering in the North Atlantic trade winds, *Nature, 380*, 416–419, 1996.

Li-Jones, X., and J. M. Prospero, Variations in the size distribution of non-sea-salt sulfate aerosol in the marine boundary layer at Barbados: Impact of African dust, *J. Geophys. Res., 103*, 16,073–16,084, 1998.

Liousse, C., J. E. Penner, C. Chuang, J. J. Walton, and H. Eddleman, A global three-dimensional study of carbonaceous aerosol, *J. Geophys. Res., 101*, 19,411–19,432, 1996.

Liu, X., P. Van Espen, F. Adams, J. Cafmeyer, and W. Maenhaut, Biomass burning in Southern Africa: Individual particle characterization of atmospheric aerosols and savanna fire samples, *J. Atmos. Chem., 36*, 135–155, 2000.

McInnes, L. M., P. K. Quinn, D. S. Covert, and T. L. Anderson, Gravimetric analysis, ionic composition, and associated water mass of the marine aerosol, *Atmos. Environ., 30*, 869–884, 1996.

McInnes, L., M. Bergin, J. Ogren, and S. Schwartz, Apportionment of light scattering and hygroscopic growth to aerosol composition, *Geophys. Res. Lett., 25*, 513–516, 1998.

Neusüss, C., D. Weise, W. Birmili, H. Wex, A. Wiedensohler, and D. S. Covert, Size-segregated chemical, gravimetric and number distribution-derived mass closure of the aerosol in Sagres, Portugal during ACE-2, *Tellus, 52*, 169–184, 2000.

Patterson, E. M., and C. K. McMahon, Absorption characteristics of forest fire particulate matter, *Atmos. Environ., 18*, 2541–2551, 1984.

Patterson, E. M., D. A. Gillette, and B. H. Stockton, Complex index of refraction between 300 and 700 nm for Saharan aerosols, *J. Geophys. Res., 82*, 3153–3160, 1977.

Pilinis, C., and J.H. Seinfeld, Continued development of a general equilibrium model for inorganic multicomponent atmospheric aerosols, *Atmos. Environ., 21*, 2453–2466, 1987.

Pitzer, K. S. and G. Mayorga, Thermodynamics of electrolytes, II, Activity and osmotic coefficients for strong electrolytes with one or both ions univalent, *J. Phys. Chem., 77*, 2300–2308, 1973.

Quinn, P. K., and D. J. Coffman, Local closure during ACE 1: Aerosol mass concentration and scattering and backscattering coefficients, *J. Geophys. Res., 103*, 16,575–16,596, 1998.

Quinn, P. K., V. N. Kapustin, T. S. Bates, and D. S. Covert, Chemical and optical properties of marine bound-

ary layer aerosol particles of the mid-Pacific in relation to sources and meteorological transport, *J. Geophys. Res., 101*, 6931–6951, 1996.

Quinn, P. K., D. J. Coffman, V. N. Kapustin, T. S. Bates, and D. S. Covert, Aerosol optical properties in the marine boundary layer during ACE 1 and the underlying chemical and physical aerosol properties, *J. Geophys. Res., 103*, 16,547–16,563, 1998.

Quinn, P. K., and D. J. Coffman, Comment on "Contribution of different aerosol species to the global aerosol extinction optical thickness: Estimates from model results" by Tegen et al. [1997], *J. Geophys. Res., 104*, 4241–4248, 1999.

Quinn, P. K., et al., Surface submicron aerosol chemical composition: What fraction is not sulfate?, *J. Geophys. Res., 105*, 6785–6806, 2000.

Reynolds, R. M., M. A. Miller, and M. J. Bartholomew, Design, operation, and calibration of a shipboard fast-rotating shawdowband radiometer, *J. Atmos. Oceanic Technol., 18*, 200–214, 2001.

Robinson, R. A., and R. H. Stokes, *Electrolyte Solutions*, 2nd ed., Butterworths, London, 1965.

Roth, B., and K. Okada, On the modification of sea-salt particles in the coastal atmosphere, *Atmos. Environ., 32*, 1555–1569, 1998.

Russell, P. B., P. V. Hobbs, and L. L. Stowe, Aerosol properties and radiative effects in the United States East Coast haze plume: An overview of the Tropospheric Aerosol Radiative Forcing Observational Experiment (TARFOX), *J. Geophys. Res., 104*, 2213–2222, 1999.

Savoie, D. L., and J. M. Prospero, Water-soluble potassium, calcium, and magnesium in the aerosols over the tropical North Atlantic, *J. Geophys. Res., 85*, 385–392, 1980.

Seinfeld, J. H., and S. N. Pandis, *Atmospheric Chemistry and Physics*, John Wiley, New York, 1998.

Smirnov, A., O. Yershov, and Y. Villvalde, Measurement of aerosol optical depth in the Atlantic Ocean and Mediterranean Sea, in *Atmospheric Sensing and Modelling II*, edited by R. P. Santer, *Proc. SPIE Int. Soc. Opt. Eng., 2582*, 203–213, 1995.

Sokolik, I. N., and O. B. Toon, Incorporation of mineralogical composition into models of the radiative properties of mineral aerosol from UV to IR wavelengths, *J. Geophys. Res., 104*, 9423–9444, 1999.

Spinhirne, J. D., J. Rall, and V. S. Scott, Compact eye-safe lidar systems, *Rev. Laser Eng., 23*, 26–32, 1995.

Stelson, A. W., Urban aerosol refractive index prediction by partial molar refraction approach, *Environ. Sci. Technol., 24*, 1676–1679, 1990.

Stratman, F., and A. Wiedensohler. A new data inversion algorithm for DMPS measurements, *J. Aerosol Sci., 27*, 339–340, 1997.

Tang, I. N., Chemical and size effects of hygroscopic aerosols on light scattering coefficients, *J. Geophys. Res., 101*, 19,245–19,250, 1996.

Tang, I. N., and H. R. Munkelwitz, Simultaneous determination of refractive index and density of an evaporating aqueous solution droplet, *Aerosol Sci. Technol., 15*, 201–207, 1991.

Tang, I. N., and H. R. Munkelwitz, Water activities, densities, and refractive indices of aqueous sulfates and sodium nitrate droplets of atmospheric importance, *J. Geophys. Res., 99*, 18,801–18,808, 1994.

Tang, I. N., A. C. Tridico, and K. H. Fung, Thermodynamic and optical properties of sea-salt aerosol, *J. Geophys. Res., 102*, 23,269–23,275, 1997.

Tangren, C. D., Scattering coefficient and particulate matter concentration in forest fire smoke, *J. Air Pollut. Control Assoc., 32*, 729–732, 1982.

Turpin, B. J., and H. Lim, Species contribution to PM2.5 concentrations: Revisiting common assumptions for estimating organic mass, *Aerosol Sci. Technol.*, in press, 2000.

Turpin, B. J., J. J. Huntzicker, and S. V. Hering, Investigation of organic aerosol sampling artifacts in the Los Angeles Basin, *Atmos. Environ., 28*, 23,061–23,071, 1994.

Turpin, B. J., P. Saxena, and E. Andrews, Measuring and simulating particulate organics in the atmosphere: Problems and prospects, *Atmos. Environ., 34*, 2983–3013, 2000.

Voss, K. J., E. Welton, P. Quinn, R. Frouin, M. Reynolds, and M. Miller, Aerosol optical depth measurements during the Aerosols99 experiment, *J. Geophys. Res.*, this issue (a).

Voss, K. J., E. J. Welton, J. E. Johnson, A. M. Thompson, P. K. Quinn, and H. Gordon, Lidar measurements during Aerosols99, *J. Geophys. Res.*, this issue (b).

Wiedensohler, A., et al., Intercomparison study of the size-dependent counting efficiency of 26 condensation particle counters, *Aerosol Sci. Technol., 27*, 224–254, 1997.

Zdanovskii, A. B., *Tr. Solyanoi Lab. Vses. Inst. Galurgii Akad. Nauk SSSR*, no. 6, 1936.

T. S. Bates, D. J. Coffman, J. E. Johnson, T. L. Miller, and P. K. Quinn, Pacific Marine Environmental Laboratory, NOAA, 7600 Sand Point Way NE, Seattle, WA 98115-6349. (quinn@pmel.noaa.gov)

C. Neusüss, Institute for Tropospheric Research, Permoserstr. 15, 04318 Leipzig, Germany.

K. Voss, Department of Physics, University of Miami, Miami, FL 33149.

E. J. Welton, NASA, Goddard Earth Science and Technology Center, University of Maryland, Greenbelt, MD 20771.